

1 Relevance of acoustic methods to quantify bedload transport 2 and bedform dynamics in a large sandy-gravel bed river

3 Jules Le Guern¹, Stéphane Rodrigues^{1,2}, Thomas Geay³, Sébastien Zanker⁴, Alexandre Hauet⁴,
4 Pablo Tassi^{5,6}, Nicolas Claude^{5,8}, Philippe Jugé⁷, Antoine Duperray¹, Louis Vervynck¹.

5 ¹UMR CNRS CITERES, University of Tours, France.

6 ²Graduate School of Engineering Polytech Tours, University of Tours, France.

7 ³BURGEAP R&D, Grenoble, France.

8 ⁴EDF, Division Technique Générale, Grenoble, France.

9 ⁵EDF R&D – National Laboratory for Hydraulics and Environment (LNHE), Chatou, France.

10 ⁶Saint-Venant Laboratory for Hydraulics, Chatou, France.

11 ⁷CETU Elmis Ingénieries, University of Tours, Chinon, France.

12 ⁸EDF, Centre Ingénierie Hydraulique, La Motte Servolex, France.

13 *Correspondence to:* Jules Le Guern (leguern@univ-tours.fr).

14 Abstract

15 Despite the inherent difficulties in quantifying its value, bedload transport is essential for understanding
16 fluvial systems. In this study, we assessed different indirect bedload measurement techniques with a
17 reference direct bedload measurement in a reach of a large sandy-gravel bed river. Acoustic Doppler
18 Current Profiler (aDcp), Dune Tracking Method (DTM) and hydrophone measurement techniques were used
19 to determine bedload transport rates by using calibration with the reference method or by using empirical
20 formulas. This study is the first work which attempted to use a hydrophone to quantify bedload rates in a
21 large sandy-gravel bed river. Results show that the hydrophone is the most efficient and accurate method
22 for determining bedload fluxes in the Loire River. Although further work is needed to identify the
23 parameters controlling sediment self-generated noise, the calibration procedure adopted in this study
24 allows a satisfactory estimation of bedload transport rates. Moreover, aDcp and hydrophone measurement
25 techniques are accurate enough to quantify bedload variations associated with dune migration.

Supprimé: to quantify

Supprimé: to understand

Supprimé: to determine

Supprimé: to

26 1. Introduction

27 Worldwide, rivers are in crisis (Vörösmarty et al., 2010). While changes in flow characteristics and fragmentation
28 are well known (Grill et al., 2019), the impacts of human activities on the sediment budgets are yet
29 underrepresented (Kondolf et al., 2018). The quantification of bedload transport is a key element to understand,
30 manage and restore the physical and ecological functioning of fluvial systems. It is a prerequisite to an accurate
31 estimation of global sediment budgets delivered by rivers to oceans (Syvitski and Milliman, 2007), to better
32 understand bedform dynamics in river channels (Best, 1988; Bertoldi et al., 2009; Rodrigues et al., 2015; Claude

37 et al., 2014) and to reproduce satisfactorily morphodynamic processes with numerical modelling (Mendoza et al.
38 2017; Cordier et al., 2020).

39 However, in large rivers, this parameter remains difficult to estimate mainly due to human and material resources
40 required to collect accurate measurements. Among the available tools, indirect measurement techniques are
41 promising alternatives to direct measurements that are often cumbersome to implement, and can be time-
42 consuming and perilous (Gray et al., 2010). Since the 2000s, numerous studies have been carried out to process
43 the signal captured by acoustic Doppler current profilers (aDcp) as a tool for determining the apparent bedload
44 velocity (Rennie et al., 2002; Rennie and Villard, 2004; Rennie and Millar, 2004; Kostaschuk et al., 2005; Villard et
45 al., 2005; Gaeuman and Jacobson 2006; 2007; Holmes et al., 2010; Ramooz and Rennie, 2010; Latosinski et al.,
46 2017; Conevski et al., 2019; Conevski et al., 2020a). The use of passive acoustic instruments has also been widely
47 used to quantify bedload transport. Even though these latter techniques have been developed through the
48 application of measurement tools such as geophones or hydrophones, their domain of applicability is restricted to
49 the study of rivers with coarse sediments (Barton et al., 2010; Hilldale et al., 2014; Marineau et al., 2016; Geay et
50 al., 2017). This study aims to develop the use of passive acoustic technique in large sandy-gravel bed rivers for
51 quantifying bedload rates and bedforms dynamics.

52 In sandy-gravel bed rivers, the presence of bedforms is generally used to indirectly estimate bedload transport
53 (Simons et al., 1965). Single beam (Peters, 1978; Engel and Lau, 1980) or multibeam echosounders (Nittrouer et
54 al., 2008; Leary and Buscombe, 2020) are tools usually adopted to determine morphological parameters (such as
55 bedform height, wavelength and celerity) or to estimate sediment budget (Frings et al., 2014). These bathymetrical
56 surveys are often carried out simultaneously with sediment sampler measurements (Gaeuman and Jacobson,
57 2007; Claude et al., 2012) to calibrate the signal with a direct reference although the latter are intrusive and
58 characterized by a low spatial representativeness. These drawbacks can therefore limit the applicability of these
59 measurement techniques, in particular for large lowland rivers.

60 In this work, we compare the efficiency of active and passive acoustic techniques to quantify bedload transport.
61 The investigation took place in a reach of the Loire River (France), which is characterized by a sandy gravel bed
62 evolving through bars and superimposed dunes migration (Le Guern et al., 2019b).

63 The main objectives of this study were: 1) to compare indirect methods for estimating bedload with bedload
64 estimates based on physical samples; 2) to estimate the accuracy of acoustic methods to measure cross sectional
65 variations of bedload fluxes for various discharge conditions; and 3) to investigate the capabilities of hydrophones
66 and aDcps at capturing bedload variations along bedforms.

Supprimé: were proposed

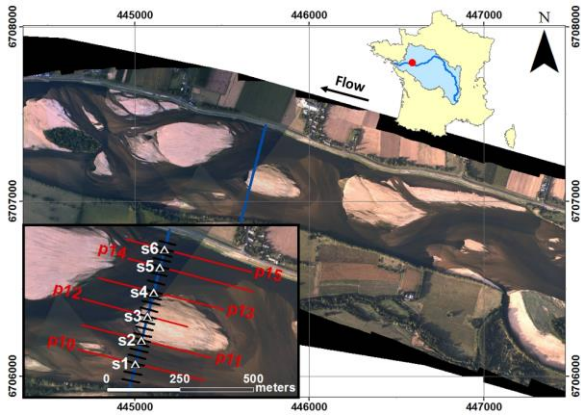
Supprimé: techniques

Supprimé: the presence of migrating

70 2. Study site

71 The study site is located near Saint-Mathurin-sur-Loire, in the lower reach of the Loire River (France), approximately
72 150 km upstream of the mouth of the Loire River. The study reach is 2.5 km long, 500 m wide, nearly straight, with
73 a bed slope of 0.02 % (Fig. 1). During this work we measured the grain size distribution and flow characteristics at
74 different locations along a cross section (Fig. 1). The riverbed is composed of a mixture of siliceous sands and
75 gravels with a median diameter (D_{50}) of 0.9 mm. The D_{50} varies between 0.3 and 3.1 mm with a standard deviation
76 of 0.4 mm. The 90th percentile of the sediment grain size distribution (D_{90}) is variable with a median value of 3.3
77 mm varying from 0.5 to 15.7 mm. Hydraulic conditions varied according to discharge between 0.5 and 5.4 m for
78 the water depth, and between 0.2 and 1.4 m.s⁻¹ for the water velocity (median water depth and water velocity are
79 1.9 m and 0.9 m.s⁻¹, respectively). The width-to-depth ratio ranges from 120 to 550 depending on discharge
80 variations. The mean annual discharge at the Saumur gauging station (approx. 30 km upstream) is 680 m³.s⁻¹, with
81 a 2-years flood of 2700 m³.s⁻¹. Surveys were conducted during various hydrological conditions, with flow discharges
82 ranging from 200 to 2400 m³.s⁻¹ (Fig. 2a).

83 Bars are characterized by an average wavelength of 1300 m, corresponding to approximately three times
84 the channel width. The mean bar height is 1.5 m. At submerged conditions, bars can migrate with a celerity of 0.5 to 2
85 meters per day. During floods, the bar celerity can increase up to 4 meters per day (Le Guern et al., 2019a). During
86 floods, dunes are superimposed on bars, whose height, wavelength and mean celerity are approximately 0.3 m,
87 4.4 m and 32 meters per day, respectively.



88 Fig. 1: Aerial photographs of the study site in 2017 (courtesy of Dimitri Lague, University of Rennes, France) with
89 location of sampling points (white triangles) on the sediment transport gauging cross section (blue line), bathymetric
90 profiles (red lines) and hydrophone drifts (black lines).
91

Supprimé: It

Mis en forme : Indice

Supprimé: at the sampling points

Supprimé: with

Supprimé: and

Supprimé: the

Supprimé: 6

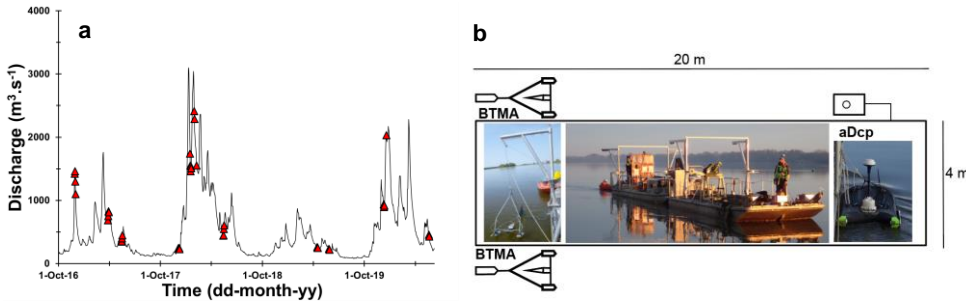
Mis en forme : Non Exposant/ Indice

Supprimé: to

Supprimé: of

100 **3. Materials and methods**

101 Direct measurements of bedload sediment transport rates were performed using pressure-difference samplers.
 102 This conventional approach was used to evaluate three indirect acoustic methods: the apparent bedload velocity
 103 assessed from aDcp measurements, the dune tracking method (DTM) inferred using single-beam echosounding,
 104 and the self-generated noise (SGN) of sediments measured using a hydrophone. A total of 72 surveys were
 105 performed from October 2016 to May 2020 (discharge ranging between 210 m³.s⁻¹ and 2290 m³.s⁻¹) including 43
 106 surveys with bedload samplers presented on Fig. 2a (Appendix A).



Supprimé: isokinetic

107
 108 Fig. 2: (a), distribution of bedload sampling surveys along the hydrograph of Saumur gauging station located about 30
 109 km upstream the study site. (b), Scheme of the main boat and disposition of monitoring facilities. Bedload Transport
 110 Meter Arnheim (BTMA) samplers: Acoustic Doppler Current Profiler (aDcp).

111 **3.1. Bedload rates obtained using pressure-difference samplers**

112 Bedload transport rates were measured using two synchronized Bedload Transport Meter Arnheim (BTMA)
 113 samplers, consisting of a sampling basket mounted on a frame. The sampling baskets have a rectangular mouth
 114 of 0.05 m high and 0.085 m wide. Complete description of the sampler can be found in de Vries (1979) or in
 115 Eijkelkamp (2003). Devices were mounted on a 20 meter-long boat stabilized using two anchors (Fig. 2b). These
 116 two samplers were deployed on 6 sampling points (S1 to S6) distributed along a cross section (Fig. 1). At each
 117 sampling point, 10 samples were collected with each BTMA (20 in total) and volumes of each samples were
 118 measured *in situ* with a graduated cone (Imhoff cone). Collected volumes were integrated over at least 2 minutes.
 119 All samples volumes from each BTMA were merged for sieving analysis (leading to 2 sediment samples per
 120 sampling point; one for each BTMA). Then, the average volume of caught sediments from the 2 BTMAs was
 121 computed and converted into instantaneous unit bedload rates as follow:

Supprimé: isokinetic

$$122 q_s BTMA = \frac{V}{b} \alpha \varepsilon \rho_s \times 10^3; \quad (1)$$

123 where $q_s BTMA$ is the unit bedload transport rate (g.s⁻¹.m⁻¹), α is the trap efficiency factor based on calibration ($\alpha=2$),
 124 V is the mean volume of the instantaneous sediment catch (m³.s⁻¹), b is instrument's mouth width ($b=0.085$ m), ρ_s

Supprimé: on

128 is the sediment density ($2650 \text{ kg}\cdot\text{m}^{-3}$) and ϵ is the volumetric sediment concentration (assumed to be equal to 0.65).
129 Suggested values of α and b were adopted from Boiten (2003) which mentioned that the trap efficiency factor does
130 not include the possible losses of sediment finer than 0.3 mm (mesh size opening). Sampler positions and sampling
131 quality were controlled by using two cameras mounted on the BTMAs but records during flood events were
132 unusable. The increase of the water depth limits the light at the bottom of the water column and the addition of a
133 mounted light did not improve the visibility because of particles in suspension. Sediment samples were analysed
134 using the standard sieving technique (Folk and Ward, 1957) to determine the grain size distribution (GSD) using
135 the tool "GRADISTAT" developed by Blott and Pye (2001). Uncertainties associated to the estimation of the unit
136 bedload were calculated following Frings and Vollmer (2017).

Supprimé: because of increasing water depth and suspension

137 3.2. Apparent bedload velocity from aDcp

138 Simultaneously with the BTMA measurements, an aDcp was installed on the boat (Fig. 2b). Measurements were
139 performed using a Sontek Riversurveyor M9 (bi-frequency, 1 and 3 MHz) or a Teledyne RD Instruments Rio Grande
140 (1.2 MHz). The sampling time needed to get a stable apparent velocity is in the range of 3 min for the case without
141 bedforms (Conevski et al., 2019) and 25 min (Rennie et al., 2002). In our study the sampling time was between 5
142 and 190 minutes. The aDcp was coupled with a RTK GPS Magellan ProFlex 500 receiving position corrections via
143 the Teria network (centimeter level accuracy). The aDcp measurement allowed the use of both empirical approach
144 and calibration approach for comparison with sediment sampler measurements. The apparent bedload velocity V_a
145 was estimated from the bottom tracking signal, allowing the identification and the position of the river bed. In case
146 of a mobile bed, the Doppler shift of the backscattered acoustic pulse of the bottom track depends on the boat
147 velocity and to the bed velocity. According to Rennie et al. (2002), the apparent bedload velocity can be estimated
148 using:

Supprimé: range

$$149 V_a = V_{GPS} - V_{BT}; \quad (2)$$

150 where V_{GPS} and V_{BT} are the boat velocity according to GPS reference and bottom track respectively. Even if the
151 boat was anchored, the GPS signal was used in the Eq. 2 to correct apparent bedload velocity from small lateral
152 displacements observed. When the GPS signal was poor or missing, V_{GPS} was considered as null and V_a resulted
153 only from the bottom track signal V_{BT} (representing 15% of the dataset). Following Jamieson et al. (2011), the
154 apparent velocity V_a was calculated for the North and East velocity components (respectively \vec{V}_{aE} and \vec{V}_{aN}), limiting
155 the over estimation especially in areas where inconsistent directions and low magnitudes of bedload velocity were

Supprimé: to

Supprimé: the apparent velocity

Supprimé: to be

Supprimé: equal to the boat velocity according to bottom track reference because measurements were performed in a static position

$$156 \text{ found: } V_a = \sqrt{V_{aE}^2 + V_{aN}^2}.$$

157 To avoid compass and GPS issues, and to eliminate the effect of residual lateral displacement of the anchored
158 boat, the apparent bedload velocity was projected onto the flow direction using:

168 $V_{a\ proj} = V_a \cdot \cos\left(\frac{w_{dir\ BT} - b_{dir\ BT}}{180} \cdot \pi\right);$ (3)

169 with $w_{dir\ BT}$ the flow direction with bottom track reference and $b_{dir\ BT}$ the boat direction with the bottom track reference
 170 (in degree). Equation (3) gives a value of apparent bedload transport velocity for each time step (approximately
 171 equal to 1 s) that was averaged to obtain a value for each sampling point. This method assumes that bedload is
 172 orientated in the same direction as the main flow. According to Rennie et al. (2002), the bedload transport rate per
 173 unit width ($q_s\ ADCP$, $g.s^{-1}.m^{-1}$) can be computed from two different kinematic models, the first of which is:

174 $q_s\ ADCP = \frac{4}{3} \rho_s r V_{a\ proj} \times 10^3;$ (4)

175 where $r = D_{50}/2$ is the particle radius, D_{50} is the median sediment diameter (m), ρ_s is the sediment density (2650
 176 $kg.m^{-3}$). In this model, it is assumed the maximum bedload thickness is a single particle. The second model is:

177 $q_s\ ADCP = V_{a\ proj} d_s c_b \rho_s;$ (5)

178 where c_b is the concentration of the active transport layer considered as the saltation height (van Rijn, 1984), and
 179 the van Rijn (1984) formulation was adopted to compute the active layer thickness (d_s) as a function of the hydraulic
 180 condition and sediment grain size:

181 $d_s = 0.3 D_*^{0.7} T^{0.5} D_{50};$ (6)

182 $c_b = 0.18 \frac{T}{D_*} c_0;$ (7)

183 $T = \frac{(\bar{u}')^2 - (u_{cr}')^2}{(u_{cr}')^2};$ (8)

184 $\bar{u}' = \frac{\bar{u}}{5.75 \log\left(\frac{3.2d}{3D_{50}}\right)};$ (9)

185 where c_0 is the maximum bedload concentration (0.65), T is the transport stage parameter that reflects the
 186 sediment mobility, \bar{u}' is the bed shear velocity related to the grain ($m.s^{-1}$), d is the mean water depth (m), \bar{u} is the
 187 mean flow velocity measured from the aDcp ($m.s^{-1}$) and u_{cr}' is the critical bed shear velocity ($m.s^{-1}$) calculated from
 188 the Shields curve (Van Rijn, 1984) and function of grain size through the scaled particle parameter D_* :

189 $D_* = D_{50} \left[\frac{(s-1)g}{\nu^2} \right]^{\frac{1}{3}};$ (10)

190 where g is the acceleration of the gravity ($m.s^{-2}$), ν is the kinematic viscosity ($m^2.s^{-1}$) and s the sediment density
 191 ratio. For the range of grain size of this study, u_{cr}' is computed as follows:

192 $10 < D_* \leq 20; u_{cr}' = [0.04 D_*^{0.1} (s-1)g D_{50}]^{0.5};$ (11)

193 $20 < D_* \leq 150; u_{cr}' = [0.013 D_*^{0.29} (s-1)g D_{50}]^{0.5};$ (12)

194 In order to evaluate the sensibility of the apparent bedload post-processing, the two kinematic models (Eq. 4 and
 195 Eq. 5) were tested using raw apparent bedload velocity (V_a) and projected apparent bedload velocity ($V_{a\ proj}$).

196 To assess the capability of the aDcp to detect bedforms through the evolution of apparent bedload velocity, 3
 197 surveys were conducted by positioning the aDcp 0.6 m above the river bed. This experimental scheme was adopted

Supprimé: than

Supprimé: namely

Supprimé:

Supprimé: and

202 to avoid lateral movements of the boat, to be as close as possible to the river bed, and to reduce the space between
203 beams. This configuration permitted us to fix the footprint for each beam to about 0.0046 m² and a distance of 0.56
204 m between opposed beams. This allowed us to describe the apparent bedload velocity with a finer accuracy
205 especially in the presence of bedforms of 0.2 m height and 3.9 m long (in average). These surveys were performed
206 for several hours (from 2.1 h to 4.7 h) to capture the migration of more than one dune lee side passing under the
207 device. The value of apparent bedload velocity was smoothed by using a moving windows with an average of 500
208 points (approximately 500 seconds) to remove the outliers from the raw dataset. In the present study, all negative
209 values were excluded from the comparison with BTMA measurements (16% of apparent velocity values).

210 3.3. Bathymetrical echosounding and dune tracking method

211 A single beam echosounder Tritech PA500 (0.5 kHz) coupled with a RTK GPS LEICA Viva GS25 was used for
212 high-frequency bathymetric surveys to determine bar and dune morphodynamics along 6 longitudinal profiles
213 (about 400 m long) centred on sampling points indicated in Fig. 1. Dune height (H_D) and wavelength (λ_D) were
214 estimated using the Bedform Tracking Tool (BTT) based on the zero-crossing method (Van der Mark and Blom,
215 2007). Dune celerity (C_D) was estimated with the Dune Tracking Method (DTM, Simons et al., 1965; Engel and
216 Lau, 1980) following the dune crests between two subsequent bathymetric surveys for a mean interval time equal
217 to 40 minutes. The interval time needs to be adjusted with discharge because of the dune celerity variation from
218 one survey to another. The determination of a proxy to evaluate sediment transport directly from DTM
219 measurements is difficult because dune migration is function of several parameters. A semi-empirical equation that
220 accounts for these parameters was used to compare bedload transport rates with the reference measurement. The
221 computed dune parameters were used to calculate the unit bedload transport rate (q_s^{DTM} , g.s⁻¹.m⁻¹) using the
222 formula by Simons et al. (1965):

$$223 q_s^{DTM} = (1-\lambda) \rho_s H_D C_D \beta \times 10^3; \quad (13)$$

224 where H_D is the mean dune height along the profile (m), C_D is the median dune celerity (m.s⁻¹) and β is the bedload
225 discharge coefficient equal to 0.5 for a perfect triangular dune shape. The β coefficient neglects the volume of
226 bypassing material from previous dunes or exchanges between bedload and suspended load (Wilbers, 2004). Due
227 to its large variability (Van den Berg, 1987; Ten Brinke et al., 1999; Wilbers, 2004), the sensibility of the bedload
228 transport rate was assessed for $\beta=[0.33; 0.57]$, as proposed by Engel and Lau (1980) and Wilbers (2004).
229 Considering the accuracy of the bathymetrical echosounding relative to the dune size, the sinuosity of dune crests,
230 and the representativeness of dune celerity, only profiles with a mean dune height greater than 0.1 m and more
231 than 10 dunes were considered.

Supprimé: were

233 3.4. Hydrophone and acoustic power

234 Passive acoustic monitoring was performed with a Teledyne RESON Hydrophone TC4014-5 (sensitivity of -180
235 dB) plugged into an EA-SDA14 card from RTSYS Company. This device has a large frequency range from 0.015
236 to 480 kHz, with a linear response until 250 kHz (± 3 dB). The beam-pattern of the hydrophone is omnidirectional.
237 The hydrophone has been deployed following the protocol proposed by Geay et al. (2020). Longitudinal profiles
238 were defined on the sediment transport sampling section (22 see Fig. 1). The boat was positioned upstream of the
239 sediment transport gauging section and left adrift at flow velocity. Depending on the water depth, the hydrophone
240 was installed at a constant depth between 0.4 and 0.7 m below the water surface. Data acquisition was stopped
241 after the boat crossed the sediment transport gauging section. The drift duration ranged between 15 to 140
242 seconds, depending on the flow velocity (mean time of 31 s). For each drift, a spectral probability density (SPD)
243 was computed (Merchant et al., 2013). Then, a median Power Spectral Density (PSD) was computed as proposed
244 by Geay et al. (2017). Median PSD are preferred to mean PSD as it filters out anomalous acoustic events such as
245 the hydrophone impinging the riverbed. The acoustic power (P) for each drift was computed by integrating the
246 median PSD over a range of frequency comprised between f_{min} (15 kHz) and f_{max} (350 kHz) (Geay et al., 2020):

$$247 P = \int_{f_{min}}^{f_{max}} PSD(f) df ; \quad (14)$$

248 The minimum frequency was chosen to avoid hydrodynamic and engine noises, while the maximum frequency was
249 set by the upper limit frequency of the device and was adjusted related to PSD. Finally, the nearest hydrophone
250 drift for each BTMA sampling point was selected. Hydrophone drifts and sampler measurements were not
251 synchronized. Several tests were carried out to ensure that these acoustic power variations were not related to the
252 distance between the hydrophone and the river bed. As no theoretical expression has been developed to estimate
253 bedload rates from hydrophone measurements, only the calibration approach was implemented.

254 4. Results

255 4.1. Comparison between acoustics and direct bedload transport rate measurements

256 The BTMA dataset is composed of 135 unit bedload rates calculated from 2628 individual sediment samples. This
257 dataset represents an average of 19 samples on each sampling point to compute unit bedload rates (minimum of
258 5 and maximum of 57 samples). Bedload rates measured using the BTMAs ranged between 0.01 and 268 $\text{g}\cdot\text{s}^{-1}\cdot\text{m}^{-1}$.
259 The standard deviation of unit bedload rates increased with discharge with a mean value of 33 $\text{g}\cdot\text{s}^{-1}\cdot\text{m}^{-1}$. This
260 illustrates the spatio-temporal variability of sediment transport induced by bedform migration.

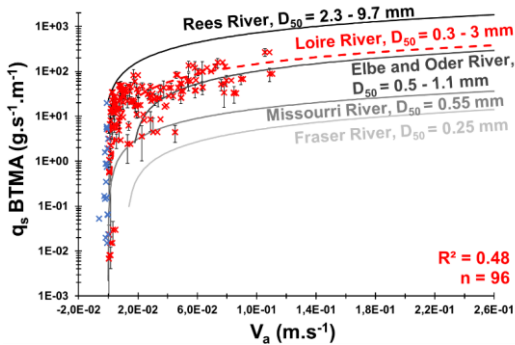
261 The aDcp dataset is composed of 96 simultaneous measurements of apparent bedload velocity and BTMA
262 samplings (Fig. 3a and Appendix B). The mean apparent bedload velocity is 0.02 $\text{m}\cdot\text{s}^{-1}$ and the maximum value

Supprimé: enables to filter

264 was $0.11 \text{ m}\cdot\text{s}^{-1}$. A Reduced Major Axis (RMA) regression has been computed between these two variables with a
 265 coefficient of determination (COD) R^2 equal to 0.51:

266 $q_s = 1456 V_a - 2.44;$ (15)

267 As shown in Fig. 3a, this site-specific calibration procedure at a reach of the Loire River is consistent with the
 268 dataset already published on several world large rivers (Rennie et al., 2017).



269
 270 Fig. 3: unit bedload transport rates measured with BTMA samplers as a function of the apparent bedload velocity
 271 measured with aDcp. Red dashed line represents the RMA regression of the Loire River. Comparison with other site-
 272 specific calibration curves (Conevski et al., 2020a; Rennie et al. 2017). Blue marks represent negative apparent bedload
 273 velocity values excluded from this regression.

274 To evaluate the accuracy of a method against a reference, the discrepancy ratio is classically employed in the
 275 literature (Van Rijn, 1984; Van den Berg, 1987; Batalla, 1997) and is defined as the ratio between the bedload rate
 276 estimated with the indirect method and the bedload rate using BTMA. Computed bedload layer volume
 277 concentration (Eq. 7) varies between 0.005 and 0.1 (0.03 in average). Bedload layer thickness (d_s) (Eq. 6) ranges
 278 between $1D_{50}$ and $7D_{50}$ ($5D_{50}$ in average). Bedload rates computed using Eq. (5) underestimate BTMA bedload
 279 rates with only 24% of the dataset with a discrepancy ratio between 0.5 and 2 (Figure 4b). By considering apparent
 280 bedload velocity without projection onto the flow direction, the kinematic model (Eq. 5) estimates satisfactorily
 281 BTMA bedload rates with 41% of the dataset with a discrepancy ratio between 0.5 and 2. Conversely, using raw
 282 apparent bedload velocity in Eq. (4), leads to only 33% of the dataset varying with a factor of 2 against 54% with
 283 projected V_a . According to these results, Eq. (4) better describes the sampler bedload rates with projected apparent
 284 bedload velocity whereas raw apparent bedload velocity are preferred with Eq. (5). Some outlier data are observed
 285 for BTMA bedload discharge lower than $0.1 \text{ g}\cdot\text{s}^{-1}\cdot\text{m}^{-1}$. These points correspond to low flow conditions for which
 286 bedload samplers could under-estimate bedload fluxes (gap between the sampler mouth and the riverbed).

Supprimé: describes fairly well

Supprimé: s

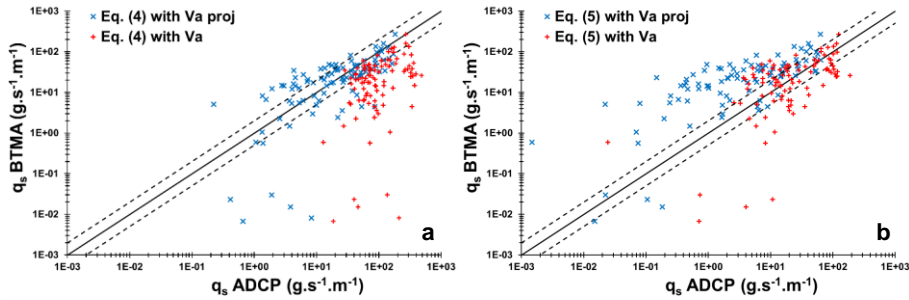
Supprimé: in

Supprimé: the

Supprimé: in

Supprimé: the

Supprimé: in the discrepancy ratio

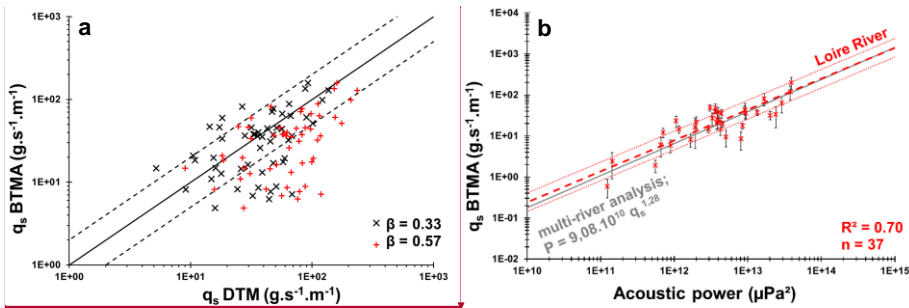


294

295 Fig. 4: log/log correlation between bedload rates measured with BTMA sampler and calculated using a) Eq. (4) and; b)
 296 Eq. (5). Solid black line represents the perfect correlation and dashed black lines represents a factor of 2 above and
 297 below the perfect correlation.

298 It appears difficult to estimate bedload rates only from dune celerity by assuming a direct relation between dune
 299 celerity and bedload transport rates measured with BTMA. Estimation of bedload transport rates from dune
 300 morphology has been performed by using empirical formula of Simons et al. (1965) (Eq. 13). The dataset is
 301 composed of 49 DTM profiles with associated BTMA samples (Appendix C). The mean dune height and length
 302 vary from 0.1 to 0.5 m, and 1.3 to 12 m, respectively. The median dune celerity varies between 13 and 61 $m \cdot d^{-1}$.
 303 According to Fig. 5a, bedload rates estimated with a discharge coefficient $\beta = 0.33$ are in agreement with BTMA
 304 bedload rates with 67% of values in a factor of 2 of the perfect correlation compared with 49% of values for a
 305 discharge coefficient of 0.57 (Fig.5a). The definition of the discharge coefficient proposed by Engel and Lau (1980)
 306 is better adapted for the observed dune shapes found in the Loire River which are characterized by mean steepness
 307 (H_D/L_D) approximately equal to 0.05 (in line with other observations on the Loire River, Claude et al., 2012;
 308 Rodrigues et al., 2015; Wintenberger et al., 2015).

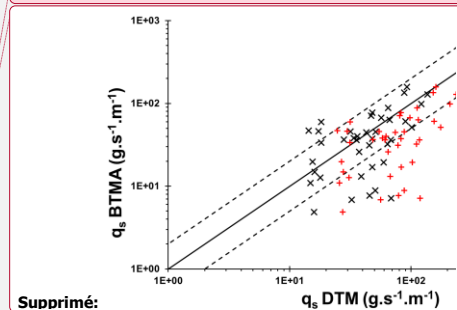
Supprimé: 4a



309

310 Fig. 5: log/log correlation between bedload rates measured with BTMA samplers and bedload rates calculated using
 311 Eq. (13). Solid black line represents the perfect correlation and dashed black lines represents a factor 2 of the perfect

Commenté [J1]: Just some missing points in the figure



Supprimé:

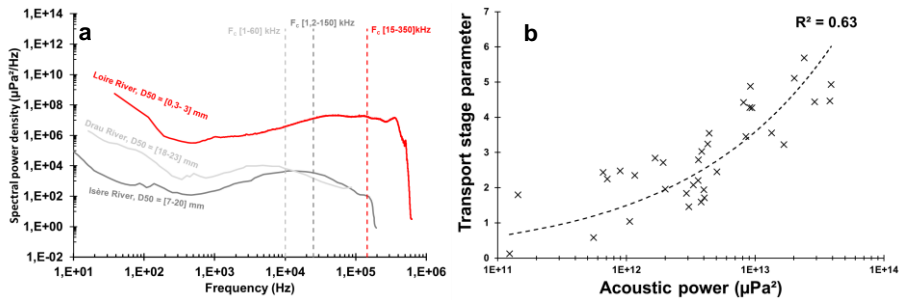
314 correlation. b), unit bedload rates measured with BTMA samplers as a function of acoustic power measured with
 315 hydrophone. Dashed red lines represents the RMA regression with envelopes curves of a factor 2 of the bedload rates.
 316 Comparison with Geay et al. (2020).

317 Even if the statistical representativeness is lower than other methods (n=37, Appendix D), the RMA regression
 318 between the acoustic power and BTMA sampling is better ($R^2=0.70$) and 60% of values varying between a factor
 319 2 (Fig. 5b). In consequence, new equation to estimate sediment transport from acoustic power is proposed:

$$320 P = 6.6 \times 10^{10} q_s^{1.32}; \quad (16)$$

321 This calibration curve is similar to observations performed by Geay et al. (2020) on 14 study sites distributed on 11
 322 different rivers despite the use of different instruments (sampler and hydrophone) and the integration of median
 323 PSD over a wider range of frequency in the present study. Moreover, the median PSD differ from the Isère River
 324 (Petrut et al., 2018) and from Drau River (Geay et al., 2017). These rivers are characterised by coarser sediments
 325 (see Fig. 6a) and the central frequency of the PSD decrease with an increasing D_{50} . These observations are in line
 326 with Thorne's (1986) theory. The central frequency of the median spectrum of the Loire River is approximately
 327 equal to 140 kHz. The frequency band of the bedload is shifted towards high frequencies due to finer grain size.

328 The acoustic power corresponding to the integration of the spectrum over a range of frequency is related to the
 329 grain size (Thorne, 1985) and sediment kinematics (Gimbert et al., 2019). To analyse the effect of sediment mobility
 330 on the acoustic power, the transport stage parameter (Van Rijn, 1984) is calculated. The power law adjusted
 331 between these two parameters provides evidence for a positive evolution of the acoustic power with sediment
 332 mobility (Fig. 6b).



333
 334 Fig. 6: (a), Comparison of PSD from 3 rivers with varying D_{50} (PSD of the Drau River and the Isère River are extracted
 335 from a single measurement, PSD of the Loire River is the median PSD from 450 measurements). (b), transport stage
 336 parameter (from Van Rijn, 1984) as a function of acoustic power.

337 The comparison can be performed between indirect methods to discuss the acceptability of the BTMA reference.
 338 The apparent bedload velocity and the acoustic power are poorly correlated with mean dune morphological
 339 parameters (Table 1).

Supprimé: are

Supprimé: ing

Supprimé: for

Supprimé: s

344 **Table 1: Coefficient of determination (COD) between dune parameters and acoustic methods (log values).**

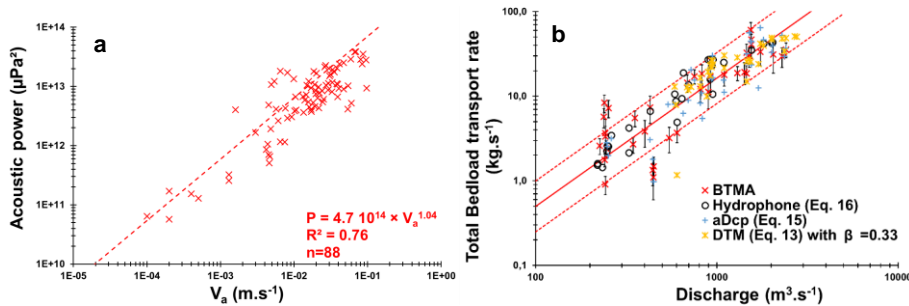
	P	V _a	q _s BTMA	H _{dune}	C _{dune}
H _{dune}	0.20	0.27	0.16	-	-
C _{dune}	0.22	0.24	0.36	0.22	-

345

346 The apparent bedload velocity estimated by aDcp is the velocity of the top layer velocity or dynamical active layer
 347 (sediment being transported over a dune), whereas the dune celerity is the mobility of the exchange event active
 348 layer, according to Church and Haschenburger (2017). It must be noted that apparent bedload velocity is higher
 349 than dune celerity by a factor approximately equal to 100. On the other hand, the apparent bedload velocity is
 350 positively correlated with the acoustic power. The COD of the RMA regression is equal to 0.76 (Fig. 7a).

351 Before focusing on the spatial distribution of unit bedload rates, total bedload rates are calculated by interpolating
 352 unit bedload rates between sampling points on the cross section for each method. The COD of the RMA regression
 353 established between BTMA bedload rates and water discharge is 0.71 (Fig. 7b) with 77% of the values varying

354 within a factor of 2. The dispersion of bedload rates is higher for low water discharge (less than the mean annual
 355 discharge of 680 m³.s⁻¹). Bedload rates are estimated from Eqs. (13), (15) and (16), for the DTM, the aDcp and the
 356 hydrophone, respectively. Both the hydrophone and DTM bedload rates are less scattered with 96% of values with
 357 a discrepancy ratio between 0.5 and 2, compared with 82% for the aDcp.



358

359 **Fig. 7: (a), acoustic power as a function of apparent bedload velocity. (b), Cross section integrated bedload transport**
 360 **rates as a function of discharge.**

361 **4.2. Spatial distribution of bedload in a sandy gravel-bed river with migrating bedforms**

362 **4.2.1. Determination of bedload transport on a cross section using acoustics methods**

363 To compare the spatio-temporal distribution of bedload transport rates, sediment transport sampling was performed
 364 on the same cross section for all surveys and for various discharge conditions. Two surveys with contrasting
 365 discharge conditions and different bed configurations are presented (Fig. 8) to illustrate the capability of acoustic,

Supprimé: mesures

Supprimé: in

Supprimé: under

Supprimé: ,

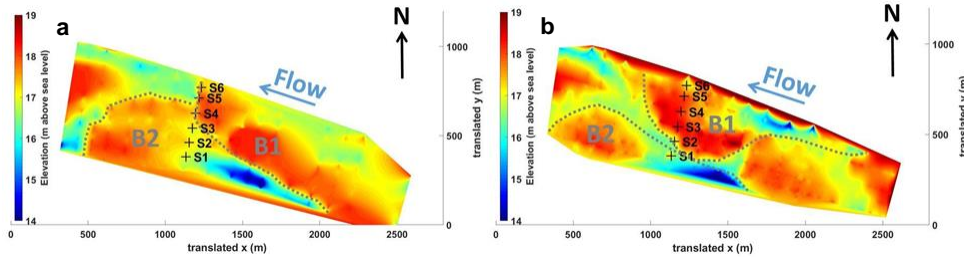
Supprimé: 800

Supprimé: in

Supprimé: the

Supprimé: s

374 methods to determine bedload active width in a river reach characterized by the presence of macroforms and
375 superimposed mesoforms (*sensu lato*, Jackson, 1975).



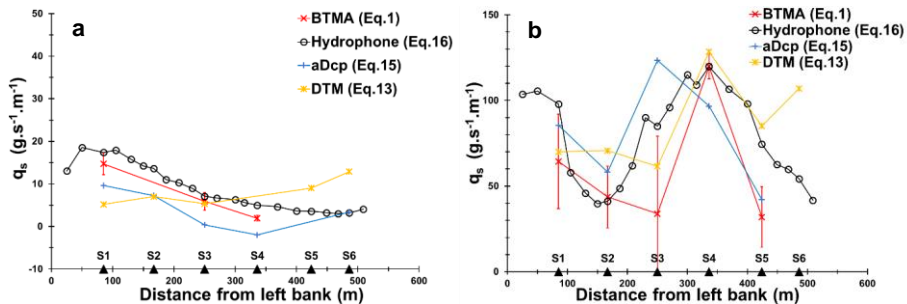
376

377 **Fig. 8: Digital Elevation Models (obtained using natural neighbours interpolation of single beam bathymetrical surveys)**
378 **showing location of sampling points with respect to bar location during: (a), survey of the 17/05/2018 ($Q=604 \text{ m}^3 \cdot \text{s}^{-1}$)**
379 **and (b), survey of the 19/12/2019 ($Q=2050 \text{ m}^3 \cdot \text{s}^{-1}$).**

Supprimé: Bathymetric

380 In May 2018, a bar (B1. Fig. 8a) was located just upstream of the sediment gauging section from the center to the
381 right part of the channel. In the left part of the channel, BTMA sampling was performed on the stoss side of another
382 bar (B2, Fig. 8a). Consequently, bedload rates gradually rose from the center of the channel ($2 \text{ g} \cdot \text{s}^{-1} \cdot \text{m}^{-1}$, S4) to the
383 left part of the channel ($15 \text{ g} \cdot \text{s}^{-1} \cdot \text{m}^{-1}$, S1) except for the DTM (Fig. 9a). The intensity of bedload transport rates was
384 evaluated for each acoustic signal from regression equations established above (Eqs. 13, 15 and 16, for DTM,
385 aDcp and hydrophone, respectively). The linear equation of aDcp calibration allow the calculation of negative,
386 bedload flux for apparent bedload velocity below $0.0016 \text{ m} \cdot \text{s}^{-1}$ (Fig. 9a, S4). ADcp and hydrophone signals followed
387 the same trend as the BTMA measurement. In the right part of the channel, no reference measurements were
388 available (S5 and S6) but all acoustic signals followed the same trend (increasing bedload transport rates). The
389 bedload rates estimated with the DTM were lower than the reference in the left part of the channel. This can be
390 explained by the reduced number of dunes in this area that caused a higher uncertainty in dune celerity
391 determination. In the right part, the proximity of the bar front induced lower bedload transport rates measured with
392 aDcp and hydrophone. DTM integrates sediment dynamics over a longitudinal profile that does not necessarily
393 reflect the bedload transport conditions at a local scale. Due to the lee effect provided by the proximity of the bar
394 front, dunes were not present downstream of the bar and only dunes located on the stoss side of the bar were used
395 to calculate the mean dune celerity. ADcp underestimates whereas the hydrophone method overestimates the unit
396 bedload rate compared with BTMA measurements.

Supprimé: s



399

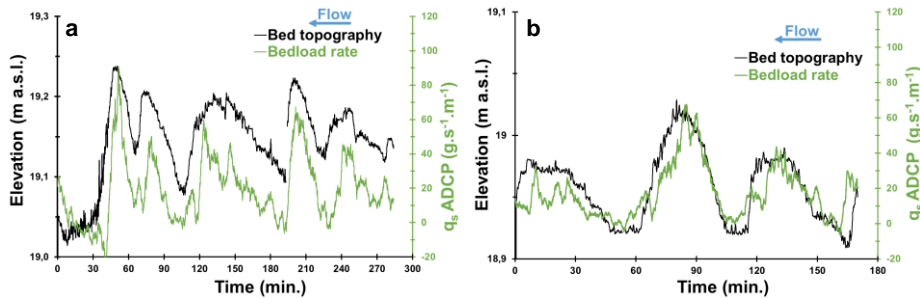
400 Fig. 9: Lateral distribution of unit bedload rates assessed from different methods for two surveys performed: (a), the
 401 17/05/2018 ($Q=604 \text{ m}^3\cdot\text{s}^{-1}$) and (b), the 19/12/2019 ($Q=2050 \text{ m}^3\cdot\text{s}^{-1}$), respectively.

402 In December 2019 (Fig. 9b), the flow discharge was higher ($2050 \text{ m}^3\cdot\text{s}^{-1}$) than the value observed in May 2018
 403 ($Q=604 \text{ m}^3\cdot\text{s}^{-1}$) and measured bedload rates ranged between 32 and $120 \text{ g}\cdot\text{s}^{-1}\cdot\text{m}^{-1}$. Due to the bar migration, the
 404 bed configuration was different. Bar B1 reached the sediment gauging cross section. As a consequence, sampling
 405 points S3 to S6 were located on the stoss side of bar B1 (Fig. 8b). The sampling point S2 was located just
 406 downstream of the bar front where the velocity and sediment transport rates were lower (Fig. 8b). The high spatial
 407 resolution of the hydrophone measurements confirmed that the preferential bedload active width was located
 408 between 250 and 450 m from the left bank (Fig. 9b). For this survey, acoustic signals (*i.e.* acoustic power, apparent
 409 bedload velocity) followed the same evolution pattern as samplers along the cross section except for S3. Bedload
 410 transport rates determined with the DTM did not follow the trend of bedload rates determined with aDcp and
 411 hydrophone at the proximity of bar front and near the bank as in the previous survey (S2 and S6). The hydrophone
 412 model overestimated the sediment transport in comparison with the BTMAs for S1, S3 and S5.

413 4.2.2. Sediment transport processes on bedforms analyzed from aDcp and hydrophone

414 The aDcp computed bedload rates evolved according to bedform location for fixed measurements performed on
 415 dunes of height ranging between 0.05 m and 0.2 m (Fig. 10a and 10b). Higher bedload rates were found on the
 416 crest of the dune and lower values in the trough. The amplitude of bedload rates between crest and trough for low
 417 flow conditions (Fig. 10b) ranged between $42 \text{ g}\cdot\text{s}^{-1}\cdot\text{m}^{-1}$ and $67 \text{ g}\cdot\text{s}^{-1}\cdot\text{m}^{-1}$. For higher flow conditions, it varied between
 418 $45 \text{ g}\cdot\text{s}^{-1}\cdot\text{m}^{-1}$ and $91 \text{ g}\cdot\text{s}^{-1}\cdot\text{m}^{-1}$ (Fig. 10a). These values were extracted considering bedload rates in trough as equal
 419 to zero (not negative). The aDcp linear regression (Eq. 15) did not allow the calculation of bedload transport rates
 420 due to negative apparent bedload velocity. This is the case downstream the lee face of dunes (Fig. 10a, between
 421 8 to 42 min., 96 to 107 min., 185 to 193 min., and 227 to 230 min.; Fig. 10b, between 48 to 55 min. and 153 to 162
 422 min.). The mean time recorded between two successive dune crests was 1 hour.

Supprimé: values

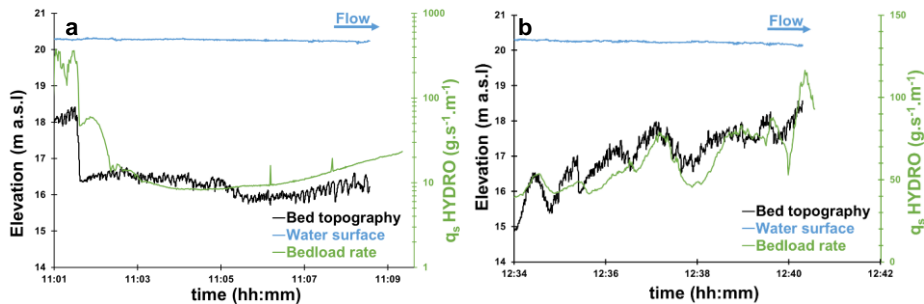


424

425 Fig. 10: Bedload rates calculated using Eq. (15) and bed topography obtained during a static measurement performed
 426 using an aDcp. (a), survey done on the 20/05/2020 ($Q=470 \text{ m}^3 \cdot \text{s}^{-1}$; mean water depth = 1.04 m) and (b), survey done on
 427 the 29/05/2019 ($Q=210 \text{ m}^3 \cdot \text{s}^{-1}$; mean water depth = 0.85 m).

428 Hydrophone drifts showed that the longitudinal evolution of acoustic power can be correlated with changes in
 429 elevation of the riverbed due to dune and bar presence. For instance, in the presence of a 2 meter high bar front,
 430 the bedload rate significantly decreased, illustrating the lee effect that is characterised by a decrease in bedload
 431 sediment transport (Fig. 11a). This shows that the hydrophone is sensitive enough to detect this local phenomenon
 432 induced by the presence of a bar front immediately upstream. The bedload rates range from about $8 \text{ g} \cdot \text{s}^{-1} \cdot \text{m}^{-1}$ on
 433 the bar crest to $376 \text{ g} \cdot \text{s}^{-1} \cdot \text{m}^{-1}$ in the bar trough ($1 \cdot 10^{12} \text{ } \mu\text{Pa}^2$ to $1.7 \cdot 10^{14} \text{ } \mu\text{Pa}^2$ of acoustic power, respectively).
 434 According to flow velocity measurements, it appears that a 2 m high bar front can influence flow velocity and
 435 bedload transport rates up to the reattachment point located approximately 100 m downstream. Downstream of the
 436 bar front, the bedload transport rate increased at 11h06min (Fig. 11a) that would be in coincidence with the flow
 437 reattachment point. Further downstream, the bedload transport rate increased from 8.5 to $23.4 \text{ g} \cdot \text{s}^{-1} \cdot \text{m}^{-1}$
 438 (representing respectively an acoustic power of $1.2 \cdot 10^{12} \text{ } \mu\text{Pa}^2$ to $4.1 \cdot 10^{12} \text{ } \mu\text{Pa}^2$), where dunes exhibit a more
 439 regular shape increasing their amplitudes from 0.02 m to 0.4 m, approximately. On the left part of the channel (Fig.
 440 11b), the drift was located at the stoss side of a bar where larger dunes were observed (about 1 m in height) with
 441 superimposed small dunes (height approximately equal to 0.3 m). The bedload transport rate calculated above
 442 these bedforms increased near the crests of the large dunes (about $80 \text{ g} \cdot \text{s}^{-1} \cdot \text{m}^{-1}$) and decreased in the troughs
 443 (about $50 \text{ g} \cdot \text{s}^{-1} \cdot \text{m}^{-1}$) where superimposed bedforms were smaller (Fig. 11b).

Supprimé: from



445

446 Fig. 11: Bedload rates calculated on bedforms using the hydrophone and Eq. (16) near a bar front (a) and on a dune
 447 field (b). Bed topography and water surface along two longitudinal bathymetric profiles for the 08/02/2018 survey,
 448 $Q=1550 \text{ m}^3 \cdot \text{s}^{-1}$: (a), P10, mean water depth = 3.8 m. The profile length from 11:01 to 11:09 corresponds to 400 m; (b),
 449 P12, mean water depth = 3.4 m. The profile length from 12:34 to 12:41 corresponds to 518 m.

450 5. Discussion

451 5.1. Relevance of acoustics for computing bedload transport rates

452 Despite their lack of accuracy and their low spatial representativeness, samplers allow a direct measurement of
 453 bedload and represents the only reference measurement of bedload in the field. The presence of bars affect
 454 sediment transport locally and make sampling method very sensitive to the location of the sampling point. For low
 455 water discharge (below mean annual discharge, $800 \text{ m}^3 \cdot \text{s}^{-1}$), bars are emerged and reduce considerably the width
 456 where sediment transport occurs. The number of sampling point decreases with discharge (because bars were not
 457 flooded) leading to a higher bedload rates variability (Fig. 7b). Moreover, in weak bedload transport conditions, the
 458 BTMA sampler most likely performed with reduced efficiency initially calibrated to 50%, (van Rijn and Gaweesh,
 459 1992; Gaweesh and van Rijn, 1994; Banhold et al., 2016). The presence of dunes influences the performance of
 460 the sampler by preventing the exact positioning of sampler mouth on the river bed. These deficiencies lead to a
 461 large uncertainty in bedload estimation which set the limits of the comparison with other methods.

462 The use of hydrophones to estimate bedload transport in a lowland sandy gravel-bed river constitutes a new
 463 research topic. As discussed by several authors, the use of hydrophones was so far restrained to gravel-bed rivers
 464 (Bedeus and Ivicsics, 1963; Barton et al., 2010; Hilldale et al., 2014; Thorne, 2014; Marineau et al., 2016; Geay et
 465 al., 2017) or marine environments (Thorne et al., 1984; Thorne, 1986; Blanpain et al., 2015). More recently, Geay
 466 et al. (2020) highlighted that the acoustic power measured with a hydrophone can be correlated to the sampler
 467 measurements of bedload in fluvial environments characterized by bed slopes varying between 0.05 and 2.5% and
 468 channel width ranging between 8 and 60 m. In these mountainous environments, the median grain size ranged
 469 between 0.9 and 62 mm ($n=582$ samples). In our study, the downstream reach of the Loire River shows smaller

Supprimé: s

471 slope ($S=0.02\%$), a wider channel ($W=500$ m), and a median grain size ranging between 0.3 mm to 3.1 mm ($n=450$
472 samples). The hydrophone is therefore an efficient tool for sediment transport gauging, allowing the measurement
473 of numerous sampling points (average of 17 sampling points) during a relatively shorter time period (one hour).
474 This high spatial discretization makes the hydrophone functional over a wide range of discharges (even for low
475 water discharge, Fig. 6b) by catching the high spatial variability of bedload transport. It should be pointed that the
476 regression calculated in the present study (Eq. 16) is obtained from unit bedload rates (from several samples) and
477 the acoustic power resulting to a unique acoustical drift, whereas Geay et al. (2020) compared averaged cross
478 section bedload rates and acoustic power. Despite these differences, the data presented above corroborate the
479 results by Geay et al. (2020) and support their conclusions concerning the determination of a global calibration
480 curve between acoustic power and bedload rates by extending its application to the lowland sandy gravel-bed
481 rivers. Although this needs to be confirmed by further investigations to better understand parameters that control
482 the acoustic power measured (such as the propagation of sound waves in water (Geay et al., 2019) and their
483 attenuation, the saltation length and associated impact celerity, or sediment grain size), results presented in this
484 study suggest that the hydrophone method could be an efficient way to measure and to map bedload transport
485 rates on a wider range of fluvial systems.

486 Several laboratory studies have been carried out (Ramooz and Rennie, 2010; Conevski et al., 2019; Conevski et
487 al., 2020b) and rivers instrumented with aDcp to determine bedload rates (Rennie et al., 2002; Rennie and Millar,
488 2004; Gaeuman and Jacobson, 2006; Gaeuman and Pittman, 2010; Brasington et al., 2011; Conevski et al.,
489 2020a). Recent works have been carried out on two rivers (Elbe, Oder) similar to the Loire River in term of grain
490 size characteristics, flow and shear velocity, and water depth (Conevski et al., 2020a). Even if the correlation
491 between apparent bedload velocity and bedload rates is significant, this calibration equation (Eq. 15) was obtained
492 from two very similar rivers. Despite these observations, there is no general agreement between bedload rates and
493 apparent velocity (Rennie and Villard, 2004; Rennie et al., 2017). The response of aDcp to bedload transport
494 depends on several parameters The variation of the impulse frequency, the pulse length, beam focusing or
495 associated internal signal processing (Broadband or Narrowband) can lead to different estimation of the apparent
496 bedload velocity for the same sediment transport conditions (Conevski et al., 2020a). These parameters vary from
497 a device to another (RDI/Sontek; Conevski et al., 2020b). As the aDcp pulse sample a volume of the riverbed
498 (Rennie et al., 2002) which can lead to a biased estimation of V_a : *i*) an underestimation in case of large roughness
499 of the riverbed with most of the reflected pulse is scattered by the immobile particles below the active layer
500 (Conevski et al., 2019); *ii*) an overestimation in case of high concentration of the bedload layer (Rennie et al., 2017)
501 or sand particles in suspension near to the riverbed (water bias, Rennie and Millar, 2004). Even if a general trend
502 seems to be highlighted by the river comparison (figure 3a) with an increasing bedload rate as grain size increases
503 for a constant V_a , the relationship between grain size and V_a cannot be easily determined in response to all variables
504 mentioned above. One explanation of this trend could be that suspended sands could contribute to the bottom

Supprimé: became

Supprimé: et

507 tracking signal without being caught by the sampler (Rennie et al., 2017). Moreover, the accuracy of the
508 measurement on a single cross section depends on the water depth heterogeneity that in turn influences the aDcp
509 footprint and makes the aDcp method location sensitive when bedforms are present (Fig. 9b). Estimation of bedload
510 rates using empirical equations is limited by the number of variables that are difficult to measure in the field (e.g.
511 thickness and concentration of active layer, Kostaschuck et al., 2005; Villard et al., 2005; Holmes, 2010; Latosinski
512 et al., 2017; Conevski et al., 2018). The results shown in Fig. 4a suggest that Eq. (4) estimates sampler bedload
513 rates if the projected bedload velocity is used. This kinematic model does not account for the thickness or the
514 sediment concentration of the bedload layer and assumes that bedload transport never exceeds the size of a single
515 particle assessed as uniform in terms of grain size (Rennie et al., 2002). These assumptions seem not to be
516 appropriate for a sandy-gravel bed river. The active layer thickness should increase as suspended bed material
517 load increases. Nevertheless, results are in agreement with BTMA bedload rates (Figure 4a). This can be explained
518 by an underestimation of the apparent bedload velocity when it is projected along flow direction. On the other hand,
519 Van Rijn (1984) defined the bedload layer thickness equal to the saltation height. The computed values of bedload
520 layer thickness are coherent with other estimations performed on comparable rivers (Conevski et al., 2020a). The
521 Eq. (5) better estimates sampler bedload rates using the raw bedload velocity (Figure 4b). If we consider that c_b
522 and d_s are well estimated by van Rijn equations (Eqs. 6 and 7), these results confirm that the projection of the
523 apparent bedload velocity decreases the bedload velocity magnitude when the bedload direction differs from flow
524 direction (e.g. bed slope effects). The influence of bedload velocity projection appears to be important when
525 bedload are computed using kinematic models. Nevertheless, the calibration curve seems to be in agreement with
526 other studies. Although, the application domain of Eq. (4) does not correspond to the conditions in the Loire River,
527 the decrease of projected V_a seems to compensate the overestimation of bedload rates when the raw apparent
528 bedload velocity is used. This is the opposite for Eq. (5) that accounts for bedload layer thickness and sediment
529 concentration. In this case, the projection of V_a leads to an underestimate of bedload rates. Further works need to
530 be done to improve the post-processing of V_a by recently published filtering procedures (Conevski et al., 2019 and
531 2020a) and to estimate its effect on calibration curve and kinematic models.

532 Contrarily to the aDcp, the DTM allows the investigation of the “event active layer” (Church and Haschenburger,
533 2017). The DTM is not a punctual measurement of bedload. Consequently, in presence of macroforms such as
534 bars, it is difficult to compare with BTMA samples because it takes into account dunes that are not necessarily
535 present at the BTMA sampling point (typically downstream of a bar lee side). To some extent, the DTM and BTMA
536 methods integrate bedload longitudinally at different scales. The presence of a local disturbance (or migrating
537 bedform at low celerity) will affect the measurement. The determination of dune celerity by post-processing is time-
538 consuming compared with the determination of dune morphology and the existing open access post-processing
539 tools. In order to determine bedload rates with empirical equations, this method needs a calibration coefficient that
540 is difficult to measure in field studies (Ten Brinke et al., 1999; Wilbers, 2004). Moreover, physical samplers sample

Supprimé: s

Supprimé: d

543 the dynamical active layer, thus are more comparable to the hydrophones and aDcps. Nevertheless, DTM remains
544 an accurate method to estimate bedload transport in the Loire River (Fig. 6b) where dunes are present and high
545 enough (over the mean annual discharge).

546 As suggested by previous authors, both aDcp (Kenney, 2006) and hydrophone (Bedeus and Ivicsics, 1963) allow
547 a reliable representation of bedload fluxes on a cross section through the regressions with bedload rates obtained
548 using samplers. Fig. 9a and Fig. 9b highlight the benefits of the use of acoustic devices for the determination of
549 bedload transport rates in a large sandy gravel-bed rivers. In the present study, the time needed in the field to
550 complete the BTMA, DTM, aDcp and hydrophone methods (respectively the red, yellow, blue and black lines of
551 Fig. 9b) are about 1 day, 4 hours, 1.5 hours and 45 minutes, respectively. These times were estimated including
552 the time needed to position and anchor the boat at each sampling point. This underlines the high potential of
553 hydrophones to quantify bedload in large rivers with high spatial variability of sediment transport and map bedload
554 sediment fluxes at a large scale as proposed by Williams et al. (2015) using the aDcp. Moreover, all indirect
555 methods tested here seem to be able to quantify total bedload transport as efficiently as the direct method (Fig. 6b)
556 but special care should be taken with local estimation of bedload rates (Fig. 9a and Fig. 9b).
557 Finally, regarding the correlation of aDcp and hydrophone with BTMA (Fig. 3a and Fig. 5b), we can raise the
558 question of the reference method. Indeed, the regression between aDcp and hydrophone is more significant
559 ($R^2=0.76$) and it could be the quality and the accuracy of BTMA sampling that reduce the quality of indirect
560 measurement regressions.

561 5.2. Hydrophone and aDcp sensitivity to bedform observations

562 Passive (hydrophone) and active (aDcp) acoustic devices are rarely used to analyse of the bedload transport rates
563 associated with bedforms in relatively large lowland rivers. Several studies mention differences in apparent bedload
564 velocity according to the location on bedforms (Rennie and Millar, 2004; Villard and Church, 2005; Gaeuman and
565 Jacobson, 2006; Holmes, 2010; Latosinski et al., 2017). These authors have shown that apparent bedload velocity
566 increases from trough to crest of the dune and confirmed previous observations made with samplers (Kostachuck
567 and Villard, 1996; Carling et al., 2000). These observations were made on large dunes that migrate too slowly to
568 allow a continuous measurement along bedforms. Our study complements these observations by providing a fixed
569 and continuous measurement of apparent bedload velocity and providing bedload transport rate estimation based
570 on a calibration curve. The mean time between two subsequent crests (1 hour) shows that even for small bedforms
571 ($H_D = 0.05$ to 0.2 m, Fig. 10a and Fig. 10b), the aDcp location significantly influences the bedload rates calculated
572 over a dune field (0.03 to 0.08 $m \cdot s^{-1}$ of difference between crest and trough). This suggests that care should be
573 taken using this method on river beds where large dunes are present but also when small dunes are migrating.
574 According to Rennie and Millar (2004), the sampling area diameter increases with the water depth and is
575 approximately equal to flow depth. Our protocol minimizes the water depth by submerging the aDcp and therefore

Supprimé: s

Supprimé: s

578 minimizes the beams sampling diameter, hence, minimizes the probability of sampling stoss or lee sides of the
579 same dune simultaneously.

Supprimé: to sample

580 In our study context, the acoustic power recorded by the hydrophone was not affected by the distance between the
581 hydrophone and the river bed. To our knowledge, there are no references mentioning investigations on bedload
582 transport rates associated with bedforms using a hydrophone. At a large time step (mean aDcp and hydrophone
583 samples), the apparent bedload velocity and the acoustic power did not follow the observed trend of mean bedform
584 characteristics derived from DTM measurement (dune celerity and dune height). This could be explained by the
585 difference of spatial scales between DTM and other methods. For a smaller time step, our results showed that
586 acoustic power is able to describe the influence of bars on bedload sediment transport (Fig. 11a). Moreover, as for
587 the aDcp, the hydrophone also detects the theoretical pattern of bedload transport rates associated with bedform
588 migration. As shown by Reesink et al. (2014), the lee effect generated by bar fronts influences the development of
589 dunes downstream. Specifically, the hydrophone is able to record the decrease of the acoustic power immediately

Supprimé: traduced

590 downstream of the bar front and its progressive increase downstream (translated by the development of dunes at
591 about 11h06, Fig. 11a). In the present study, dunes smaller than 0.4 m (Fig. 11a) were not high enough to allow
592 the observation of changes in the acoustic power along the bedform stoss sides. On the contrary, for higher dunes
593 ($H_D = 1$ m, Fig. 11b) the bedload generated noise can be well recorded by the hydrophone. A hydrophone senses
594 all noises that are propagating in the water column. Therefore, the hydrophone can record noises that are far away
595 from its location. Noises are more and more attenuated with increasing distance (Geay et al., 2019). Particularly,
596 when there is few bedload noise close to the hydrophone, the hydrophone can sense the bedload noise that are
597 generated far away. This behaviour could explain why the hydrophone tends to overestimate bedload fluxes when
598 bedload fluxes are weak especially immediately downstream of a bar front (Fig. 9b).

Supprimé: every

Supprimé: is

599 Hydrophone lower detection limit was not reached during our study whereas the dispersion of bedload rates
600 measured with samplers for low apparent bedload velocity (Fig. 3) suggests that the lower detection limit of the
601 apparent bedload velocity by the aDcp seems to be about $1 \text{ cm}\cdot\text{s}^{-1}$ (Rennie et al., 2017). This lower detection limit
602 of the apparent bedload velocity should be reduced to the bottom track uncertainty by using our protocol with a
603 submerged and fixed aDcp device.

604 6. Conclusions

605 In this work, direct (BTMA samplers), a active (aDcp and DTM) and passive (hydrophone) acoustic measurements
606 of bedload transport rates were compared in a large, sandy-gravel bed river characterized by the presence of bars
607 and superimposed dunes. Calibration curves between apparent bedload velocity measured using aDcp and
608 bedload rates measured using BTMA samplers were established but remain site-specific and dependent on grain
609 size. DTM seemed to be inappropriate where macroforms are present, as it influences the location and the size of

Supprimé: with

Supprimé: to

616 superimposed mesoforms. The calculation of bedload rates with empirical formulas is sensitive to the bedload
617 discharge coefficient for DTM and to thickness and concentration of active layer for aDcp. These parameters remain
618 difficult to measure in the field. Results presented in this study highlight the potential of the hydrophone for the
619 quantification and mapping of bedload transport rates in relatively large river channels where migrating bedforms
620 are present. Previously hydrophones have mainly been used to monitor bedload transport rates in gravel-bed rivers.
621 This study consolidates a recent study (Geay et al., 2020) by extending a general calibration curve to large sandy-
622 gravel bed rivers. The hydrophone global calibration curve allows a good representation of the bedload fluxes
623 evolution through a cross section. The method is more affordable to implement and more efficient than the
624 reference method. This might allow mapping bedload transport rates by interpolating acoustic power along several
625 cross sections performed on a large sandy gravel bed river. Moreover, acoustic devices (aDcp and hydrophone)
626 are able to capture the evolution of bedload signal along bedforms stoss and lee sides with some limitation of
627 bedform size for the hydrophone and signal noise for the aDcp. Regarding results of the comparison between
628 bedload velocity and acoustic power, the association of aDcp and hydrophone could be an efficient way to control
629 the quality of both devices. However, additional measurements and post-processing tasks are needed (Conevski
630 et al., 2019) to explore the quality of the regression in other river environments (different grain sizes, river-bed slope
631 or propagation effect).

Supprimé: while it was mainly used until today to

634 **Appendices**

635 Appendix A: BTMA dataset

636

Date	Discharge (m ³ .s ⁻¹)	Measurements type	Number of BTMA sampling points	Number of BTMA samples	Mean unit bedload rate (g.s ⁻¹ .m ⁻¹)	D ₅₀ (mm)	D ₉₀ (mm)
28/11/2016	1420	BTMA & DTM	3	50	38.1	0.8	3.0
29/11/2016	1460	BTMA & DTM	4	79	31.5	0.9	3.5
30/11/2016	1300	BTMA & DTM	4	80	33.2	0.8	2.9
01/12/2016	1100	BTMA & DTM	4	79	32.2	0.8	2.6
27/03/2017	687	BTMA. aDcp & DTM	4	80	25.3	0.7	2.9
28/03/2017	752	BTMA. aDcp & DTM	4	80	28.5	0.8	3.0
29/03/2017	827	BTMA. aDcp & DTM	4	57	29.0	0.8	3.8
30/03/2017	812	BTMA. aDcp & DTM	4	80	19.3	0.8	3.8
15/05/2017	346	BTMA. aDcp & DTM	3	60	6.3	0.9	4.8
16/05/2017	354	BTMA. aDcp & DTM	3	60	13.5	0.8	5.0
17/05/2017	401	BTMA. aDcp & DTM	3	55	9.0	0.9	4.7
18/05/2017	447	BTMA. aDcp & DTM	3	60	1.9	1.2	7.0
04/12/2017	243	BTMA & aDcp	3	60	1.8	1.1	7.4
05/12/2017	241	BTMA. aDcp & DTM	3	60	3.7	1.0	8.6
06/12/2017	243	BTMA. aDcp & DTM	3	60	6.6	1.2	6.7
07/12/2017	246	BTMA. aDcp & DTM	3	60	5.1	1.2	5.1
08/12/2017	226	BTMA. aDcp & DTM	3	60	5.0	1.6	7.9
15/01/2018	1740	BTMA. aDcp & DTM	3	60	61.4	1.0	2.9
16/01/2018	1550	BTMA. aDcp & DTM	3	60	89.4	0.9	2.8
17/01/2018	1460	BTMA. aDcp & DTM	4	80	53.2	0.8	3.0
18/01/2018	1540	BTMA. aDcp & DTM	4	80	97.7	1.0	3.3
19/01/2018	1510	BTMA. aDcp & DTM	3	60	55.6	0.8	2.6
30/01/2018	2410	BTMA. aDcp & DTM	3	60	68.6	0.8	2.3
31/01/2018	2290	BTMA. aDcp & DTM	3	59	55.8	0.8	2.2
08/02/2018	1550	BTMA. aDcp. DTM. Hydrophone	4	69	63.4	0.8	2.5
14/05/2018	443	BTMA. aDcp & DTM	4	79	2.2	0.9	2.7

15/05/2018	449	BTMA & aDcp	4	79	2.5	1.1	3.2
16/05/2018	547	BTMA. aDcp & DTM	3	60	6.6	1.2	4.4
17/05/2018	604	BTMA. aDcp. DTM. Hydrophone	3	60	7.2	1.2	4.4
15/04/2019	253	BTMA. aDcp & Hydrophone	3	60	22.1	0.9	3.3
16/04/2019	243	BTMA. aDcp & Hydrophone	3	60	22.1	1.1	5.1
17/04/2019	240	BTMA. aDcp & Hydrophone	3	60	24.9	1.2	3.7
18/04/2019	238	BTMA. aDcp & Hydrophone	3	58	16.4	1.0	5.3
27/05/2019	225	BTMA. aDcp. DTM. Hydrophone	1	26	34.6	1.0	4.8
29/05/2019	210	BTMA. aDcp. DTM. Hydrophone	1	28	22.0	1.1	3.3
09/12/2019	944	BTMA. aDcp. DTM. Hydrophone	2	40	29.1	0.7	2.5
10/12/2019	898	BTMA. aDcp. DTM. Hydrophone	3	60	20.1	0.6	2.5
11/12/2019	923	BTMA. aDcp. DTM. Hydrophone	3	45	34.9	0.8	2.4
12/12/2019	925	BTMA. aDcp. DTM. Hydrophone	2	37	26.4	0.7	2.7
19/12/2019	2050	BTMA. aDcp. DTM. Hydrophone	5	50	58.8	0.9	3.4
18/05/2020	514	BTMA & Hydrophone	1	57	19.7	0.9	2.8
19/05/2020	500	BTMA. aDcp & Hydrophone	2	79	30.9	1.0	2.6
20/05/2020	470	BTMA. aDcp & Hydrophone	4	40	14.5	-	-

637

638

639 Appendix B: ADcp dataset

640

Date	Number of aDcp sampling points	aDcp frequency (kHz)	aDcp type *1	Pulse type *2	Average aDcp sampling duration (s)	mean Va (m.s ⁻¹)	mean water depth (m)	mean flow velocity (m.s ⁻¹)
27/03/2017	4	1200	RG	BB	3909	0.013	2.0	0.7
28/03/2017	4	1200	RG	BB	3279	0.015	2.1	0.7
29/03/2017	4	1200	RG	BB	3276	0.011	2.2	0.7
30/03/2017	4	1200	RG	BB	1707	0.009	2.1	0.8
15/05/2017	3	1200	RG	BB	3018	0.002	1.3	0.8
16/05/2017	2	1200	RG	BB	2315	0.010	1.0	0.8
17/05/2017	3	1200	RG	BB	2618	0.003	1.4	0.8
18/05/2017	3	1200	RG	BB	2467	0.002	1.6	0.8
04/12/2017	3	1200	RG	BB	2647	0.000	1.2	0.7
05/12/2017	3	1200	RG	BB	2657	0.008	1.2	0.6
06/12/2017	3	1200	RG	BB	2246	0.000	1.2	0.7
07/12/2017	3	1200	RG	BB	2588	0.002	1.3	0.7
08/12/2017	3	1200	RG	BB	3400	0.003	1.2	0.6
15/01/2018	3	1200	RG	BB	3256	0.084	3.2	1.1
16/01/2018	3	1200	RG	BB	1800	0.058	2.9	1.0
17/01/2018	4	1200	RG	BB	3185	0.041	2.7	1.0
18/01/2018	4	1200	RG	BB	3656	0.055	2.8	1.0
19/01/2018	3	1200	RG	BB	2029	0.075	2.7	1.1
30/01/2018	3	1200	RG	BB	2138	0.051	3.9	1.1
31/01/2018	3	1200	RG	BB	2056	0.070	3.7	1.1
08/02/2018	4	3000	M9	BB	1136	0.038	2.8	0.9
14/05/2018	4	3000	M9	BB	2130	0.002	1.2	0.6
15/05/2018	4	variable	M9	HD	1133	0.011	1.5	0.6
16/05/2018	3	variable	M9	HD	948	0.002	1.4	0.7
17/05/2018	3	1200	RG	BB	1346	0.003	1.7	0.7
15/04/2019	3	variable	M9	HD	2601	0.009	1.2	0.8
16/04/2019	3	3000	M9	NB	1687	0.006	1.1	0.7
17/04/2019	3	variable	M9	HD	1152	0.010	1.0	0.7
18/04/2019	3	variable	M9	HD	3580	0.008	0.9	0.7

27/05/2019	1	3000	M9	NB	10949	0.003	0.9	0.8
29/05/2019	1	3000	M9	NB	11539	0.029	0.9	0.7
09/12/2019	2	3000	M9	NB	1753	0.023	1.7	0.8
10/12/2019	3	3000	M9	NB	1160	0.018	2.1	0.8
11/12/2019	3	3000	M9	NB	1288	0.027	1.6	0.9
12/12/2019	2	3000	M9	NB	1349	0.032	2.1	0.8
19/12/2019	5	3000	M9	NB	1221	0.056	3.0	1.1
19/05/2020	2	3000	M9	NB	7318	0.014	1.0	0.7
20/05/2020	4	3000	M9	NB	2988	0.004	1.6	0.7

641 *1: RG = aDcp Rio Grande RDI; M9 = aDcp M9 Sontek

642 *2 BB = Broadband (coherent Pulse); NB = Narrowband (incoherent pulse); HD = Smartpulse HD

643 ³ including sampling points with negative values.

644

645 Appendix C: DTM dataset

646

Date	Number of <u>pairs</u> of DTM profiles <u>n</u>	average interval time DTM (min)	Number of dunes	Mean H _D (m)	Mean L _D (m)	Mean C _D (m.d ⁻¹)
28/11/2016	2	18	65	0.19	2.88	43.0
29/11/2016	3	20	168	0.22	3.69	34.8
30/11/2016	3	18	121	0.24	4.16	37.6
01/12/2016	3	19	104	0.25	4.69	37.6
27/03/2017	3	38	132	0.13	3.13	28.3
28/03/2017	3	44	97	0.13	2.96	24.2
29/03/2017	3	43	117	0.14	3.25	25.7
30/03/2017	3	39	138	0.14	3.42	28.0
15/05/2017	3	65	20	0.04	2.17	18.1
16/05/2017	3	42	11	0.05	2.02	26.7
17/05/2017	3	38	18	0.05	2.01	28.0
18/05/2017	3	28	34	0.08	1.95	30.9
05/12/2017	1	73	48	0.13	2.90	17.9
06/12/2017	1	98	68	0.16	3.44	14.9
07/12/2017	1	72	63	0.17	3.62	17.3
08/12/2017	1	66	69	0.19	3.95	14.8
15/01/2018	6	23	228	0.32	6.66	38.1
16/01/2018	2	28	46	0.24	3.58	47.6
17/01/2018	3	32	52	0.25	4.36	34.9
18/01/2018	3	55	120	0.28	5.33	28.0
19/01/2018	3	31	110	0.26	4.95	31.4
30/01/2018	3	25	103	0.32	5.75	45.3
31/01/2018	4	22	83	0.28	5.02	45.4
08/02/2018	3	60	59	0.26	4.67	28.2
14/05/2018	6	35	58	0.06	2.92	20.8
16/05/2018	4	38	60	0.05	1.96	18.8
17/05/2018	6	34	81	0.05	1.98	22.3
27/05/2019	1	29	3	0.03	1.40	62.7
29/05/2019	1	26	7	0.03	1.28	30.7

09/12/2019	6	49	121	0.22	3.10	28.1
10/12/2019	6	42	227	0.17	3.60	33.2
11/12/2019	6	49	254	0.16	3.46	33.1
12/12/2019	6	50	297	0.18	3.82	35.9
19/12/2019	3	44	79	0.28	4.34	42.1

647 *1 including profiles with less than 10 dunes or mean dune celerity which could not be calculated.

648

649 Appendix D: Hydrophone dataset

650

Date	Number of Hydrophone Drifts ^{*1}	average drift duration (s)	mean acoustic power (Pa ²)
08/02/2018	24	60	2.17E+13
17/05/2018	24	80	1.46E+12
15/04/2019	11	37	1.66E+12
16/04/2019	11	42	2.25E+12
17/04/2019	11	28	1.42E+12
18/04/2019	11	30	2.35E+12
27/05/2019	8	42	5.07E+11
29/05/2019	9	36	2.00E+12
09/12/2019	22	29	6.67E+12
10/12/2019	21	22	7.69E+12
11/12/2019	22	27	8.84E+12
12/12/2019	13	27	8.97E+12
19/12/2019	22	25	2.41E+13
18/05/2020	8	50	4.53E+12
19/05/2020	8	30	3.82E+12
20/05/2020	17	36	3.07E+12

651 ^{*1} including drifts which are not at the same location of BTMA sampling points.

652

653 **Video supplement**

654 Videos of BTMA sampling were added in supplement of this manuscript to appreciate the variability of bedload in
655 the Loire River.

656 <https://doi.org/10.5446/51563>

657 <https://doi.org/10.5446/51562>

658 <https://doi.org/10.5446/51561>

659 <https://doi.org/10.5446/51560>

660 **Author contribution**

661 J. Le Guern prepared the manuscript with contributions from all co-authors. J. le Guern, T. Geay, A. Hauet, S.
662 Zanker, S. Rodrigues elaborated the experimental protocol. T. Geay developed the hydrophone signal processing
663 tools. A. Duperray P. Jugé, L. Vervynck, A. Hauet, S. Zanker, T. Geay, S. Rodrigues and J. Le Guern conducted
664 the field surveys. A. Duperray P. Jugé, and L. Vervynck performed the bathymetry post-processing. S. Rodrigues
665 and P. Tassi supervised this study. N. Claude helped in the analysis of BTMA and aDcp measurements.

666 **Competing interests**

667 The authors declare that they have no conflict of interest.

668 **Acknowledgement**

669 This study is a part of the Ph.D. thesis of the first author funded by the POI FEDER Loire (Convention no. 2017-
670 EX002207) and Agence de l'Eau Loire Bretagne (decision no.2017C005), conducted in the frame of the Masterplan
671 Plan Loire Grandeur Nature. We thank EDF DTG and ARD Intelligence des Patrimoines (Phase 2) for lending us
672 acquisition equipment. Exagone Company is acknowledged for providing us data from Teria network, Voie
673 Navigable de France (VNF) for their logistical support during field surveys and Polytech Tours. J.-P. Bakyono, P.
674 Berault, T. Bulteau, B. Deleplancouille, Y. Guerez, T. Handfus, I. Pene and C. Wintenberger, are acknowledged
675 for their help during field investigations and grain size analyses. We are grateful to T. Geay and J. Hugueny for the
676 hydrophone treatment and aDcp data post-processing tools, respectively. The authors wish to thank Pr. K. M.
677 Wantzen for checking the English quality of the manuscript.

678 **References**

- 679 Batalla, R. J.: Evaluation bed-material transport equations using field measurements in a sandy gravel-bed stream,
680 Arbúcies River, NE Spain, *Earth Surf. Process. Landforms*, 22 (2), 121-130, [https://doi.org/10.1002/\(SICI\)1096-9837\(199702\)22:2<121::AID-ESP671>3.0.CO;2-7](https://doi.org/10.1002/(SICI)1096-9837(199702)22:2<121::AID-ESP671>3.0.CO;2-7), 1997.
- 682 Banhold, K., Schüttrumpf, H., Hillebrand, G. and Frings, R.: Underestimation of sand loads during bed-load
683 measurements- a laboratory examination, in: *Proceedings of the international conference on Fluvial Hydraulics*
684 (River Flow 2016), 11-14 July 2016, Saint Louis, USA, 2406 pp., 2016.
- 685 Barton, J., Slingerland, R. R. L., Pittman, S., and Gabrielson, T. B.: Monitoring coarse bedload transport with
686 passive acoustic instrumentation: A field study, *US Geol. Surv. Sci. Investig. Rep.*, 38–51, 2010.
- 687 Bedeus, K., and Ivicsics, L.: Observation of the noise of bed load, *Gen. Assem. Comm. Hydrom. Int. Assoc. Hydrol.*
688 *Sci.* Berkeley, CA, USA, 19–31, 1963.
- 689 Bertoldi, W., Ashmore, P., and Tubino, M.: A method for estimating the mean bed load flux in braided rivers,
690 *Geomorphology*, 103, 330-340, <https://doi.org/10.1016/j.geomorph.2008.06.014>, 2009.
- 691 Best, J. L.: Sediment transport and bed morphology at river channel confluences, *Sedimentology*, 35, 481-498,
692 <https://doi.org/10.1111/j.1365-3091.1988.tb00999.x>, 1988.
- 693 Blanpain, O., Demoulin, X., Waeles, B., Ravilly, M., Garlan, T., and Guyomard, P.: Passive acoustic measurement
694 of bedload discharge features on a sandy seafloor, in: *Proceedings of Seabed and Sediment Acoustics Volume 37*
695 Part 1, Bath, United Kingdom, 7-9 september 2015.
- 696 Blott, S. J., and Pye, K.: GRADISTAT: A grain size distribution and statistics package for the analysis of
697 unconsolidated sediments, *Earth Surf. Process. Landforms*, 26 (11), 1237-1248, <https://doi.org/10.1002/esp.261>,
698 2001.
- 699 Boiten, W.: *Hydrometry*, IHE Delft Lecture Note Series, A.A. Balkema Publishers, Netherland, 256 pp,
700 <https://doi.org/10.1201/9780203971093>, 2003.
- 701 Brasington, J., Rennie, C. D., Vericat, D., Williams, R., Goodsell, B., Hicks, M., and Batalla, R.: Monitoring braided
702 river morphodynamics with an acoustic Doppler current profiler, in: *Proceedings of the 34th World Congress of the*
703 *International Association for Hydro-Environment Research and Engineering: 33rd Hydrology and Water Resources*
704 *Symposium and 10th Conference on Hydraulics in Water Engineering*, Brisbane, 3396-3403, 2011.
- 705 Carling, P. A., Williams, J. J., Gölz, E., and Kelsey, A. D.: The morphodynamics of fluvial sand dunes in the River
706 Rhine, near Mainz, Germany. II. Hydrodynamics and sediment transport, *Sedimentology*, 47, 253-278,
707 <https://doi.org/10.1046/j.1365-3091.2000.00291.x>, 2000.
- 708 Church, M., and Haschenburger, J. K.: What is the “active layer”?, *Water Resour. Res.*, 53 (1), 5-10,
709 <https://doi.org/10.1002/2016WR019675>, 2017.

710 Claude, N., Rodrigues, S., Bustillo, V., Bréhéret, J. G., Macaire, J. J., and Jugé, P.: Estimating bedload transport
711 in a large sand-gravel bed river from direct sampling, dune tracking and empirical formulas, *Geomorphology*, 179,
712 40-57, <https://doi.org/10.1016/j.geomorph.2012.07.030>, 2012.

713 Claude, N., Rodrigues, S., Bustillo, V., Bréhéret, J. G., Tassi, P., and Jugé, P.: Interactions between flow structure
714 and morphodynamic of bars in a channel expansion/contraction, Loire River, France, *Water Resour. Res.*, 50,
715 <https://doi.org/10.1002/2013WR015182>, 2014.

716 Conevski, S.: Bedload Monitoring by means of Hydro-Acoustic Techniques, Ph.D. thesis, Norwegian University of
717 Science and Technology, Norway, 200 pp., 2018.

718 Conevski, S., Guerrero, M., Ruther N., and Rennie, C. D.: Laboratory investigation of apparent bedload velocity
719 measured by ADCPs under different transport conditions, *J. Hydraul. Eng.*, 145 (11),
720 [https://doi.org/10.1061/\(ASCE\)HY.1943-7900.0001632](https://doi.org/10.1061/(ASCE)HY.1943-7900.0001632), 2019.

721 Conevski, S., Guerrero, M., Winterscheid, A., Rennie, C. D., and Ruther N.: Acoustic sampling effects on bedload
722 quantification using acoustic Doppler current profilers, *Journal of Hydraulic Research*,
723 <https://doi.org/10.1080/00221686.2019.1703047>, 2020a.

724 Conevski, S., Guerrero, M., Rennie, C. D., and Ruther, N.: Towards an evaluation of bedload transport
725 characteristics by using Doppler and backscatter outputs from ADCPs, *Journal of Hydraulic Research*,
726 <https://doi.org/10.1080/00221686.2020.1818311>, 2020b.

727 Cordier, F., Tassi, P., Claude, N., Crosato, A., Rodrigues, S., and Pham Van Bang, D.: Bar pattern and sediment
728 sorting in channel contraction/expansion area: Application to the Loire River at Bréhémont (France), *Advances in*
729 *Water Resources*, 140, <https://doi.org/10.1016/j.advwatres.2020.103580>, 2020.

730 de Vries, M.: Information on the Arnhem Sampler (BTMA), Internal Report n°3-79, Delft University of Technology,
731 Department of Civil Engineering, Fluid Mechanics Group, 1979.

732 Eijkelkamp: Operating instructions: Bedload Transport Meter Arnhem, Giesbeek, Netherland, 8 pp., 2003.

733 Engel, P., and Lau, Y. L.: Computation of Bed Load Using Bathymetric Data, *Journal of the Hydraulics Division*,
734 106 (3), 369-380, 1980.

735 Folk, R. L., and Ward, W. C.: Brazos River bar (Texas); a study in the significance of grain size parameters, *Journal*
736 *of Sedimentary Research*, 27 (1), 3-26, <https://doi.org/10.1306/74D70646-2B21-11D7-8648000102C1865D>, 1957.

737 Frings, R. M., and Vollmer, S.: Guidelines for sampling bed-load transport with minimum uncertainty,
738 *Sedimentology*, 64 (6), 1630-1645, <https://doi.org/10.1111/sed.12366>, 2017.

739 Frings, R. M., Gehres, N., Promny, M., Middelkoop, H., Schüttrumpf, H., and Vollmer, S.: Today's sediment budget
740 of the Rhine River channel, focusing on the Upper Rhine Graben and Rhenish Massif, *Geomorphology*, 204, 573-
741 587, <https://doi.org/10.1016/j.geomorph.2013.08.035>, 2014.

742 Gaeuman, D., and Jacobson, R. B.: Acoustic bed velocity and bed load dynamics in a large sand bed river, *J.*
743 *Geophys. Res.*, 111, F02005, <https://doi.org/10.1029/2005JF000411>, 2006.

744 Gaeuman, D., and Jacobson, R. B.: Field Assessment of Alternative Bed-Load Transport Estimators, *J. Hydraul.*
745 *Eng.*, 133 (12), 1319-1328, [https://doi.org/10.1061/\(ASCE\)0733-9429\(2007\)133:12\(1319\)](https://doi.org/10.1061/(ASCE)0733-9429(2007)133:12(1319)), 2007.

746 Gaeuman, D., and Pittman, S.: Relative Contributions of Sand and Gravel Bedload Transport to Acoustic Doppler
747 Bed-Velocity Magnitudes in the Trinity River, California, U.S. Geological Survey Scientific Investigations Report,
748 2010-5091, 2010.

749 Gaweesh, M. T. K., and van Rijn, L. C.: Bed-load sampling in sand-bed rivers, *J. Hydraul. Eng.*, 120 (12), 1364-
750 1384, [https://doi.org/10.1061/\(ASCE\)0733-9429\(1994\)120:12\(1364\)](https://doi.org/10.1061/(ASCE)0733-9429(1994)120:12(1364)), 1994.

751 Geay, T., Belleudy, P., Gervaise, C., Habersack, H., Aigner, J., Kreisler, A., Seitz, H., and Laronne, J. B.: Passive
752 acoustic monitoring of bed load discharge in a large gravel bed river, *J. Geophys. Res.: Earth Surf.*, 122 (2),
753 <https://doi.org/10.1002/2016JF004112>, 2017.

754 Geay, T., Michel, L., Zanker, S., and Rigby, J. R.: Acoustic wave propagation in rivers: an experimental study. *Earth*
755 *Surface Dynamics*, 7 (2), 537–548, <https://doi.org/10.5194/esurf-7-537-2019>, 2019.

756 Geay, T., Zanker, S., Misset, C., and Recking, A.: Passive Acoustic Measurement of Bedload Transport: Toward
757 a Global Calibration Curve?, *J. Geophys. Res.: Earth Surf.*, 125 (8), <https://doi.org/10.1029/2019JF005242>, 2020.

758 Gimbert, F., Fuller, B. M., Lamb, M. P., Tsai, V. C., and Johnson, J. P. L.: Particle transport mechanics and induced
759 seismic noise in steep flume experiments with accelerometer-embedded tracers, *Earth Surf. Process. Landforms*,
760 44, 219-241, <https://doi.org/10.1002/esp.4495>, 2019.

761 Gray, J. R., Gartner, J. W., Barton, J. S., Gaskin, J., Pittman, S. A., and Rennie, C. D.: Surrogate Technologies for
762 Monitoring Bed-Load Transport in Rivers, *Sedimentology of Aqueous Systems*, 46-79,
763 <https://doi.org/10.1002/9781444317114.ch2>, 2010.

764 Grill, G., Lehner, B., Thieme, M. et al.: Mapping the world's free-flowing rivers. *Nature* 569, 215–221,
765 <https://doi.org/10.1038/s41586-019-1111-9>, 2019.

766 Hilldale, R. C., Goodwillier, B. T., Carpenter, W. O., and Chambers, J. P.: Measuring Coarse Bed Load Using
767 Hydrophones, Closeout report, Reclamation Managing Water in the West, 2014.

768 Holmes, R. R. Jr.: Measurement of Bedload Transport in Sand-Bed Rivers: A Look at Two Indirect Sampling
769 Methods, U.S. Geological Survey Scientific Investigations Report, 2010-5091, 2010.

770 Jackson, R. G.: Hierarchical attributes and a unifying model of bed forms composed of cohesionless material and
771 produced by shearing flow, *Geological Society of America Bulletin*, 86, 1523-1533, 1975.

772 Jamieson, E. C., Rennie, C. D., Jacobson, R. B., and Townsend, R. D.: Evaluation of ADCP Apparent Bed Load
773 Velocity in a large Sand-Bed River: Moving versus Stationary Boat Conditions, *J. Hydraul. Eng.*, 137, 1064-1071,
774 [https://doi.org/10.1061/\(ASCE\)HY.1943-7900.0000373](https://doi.org/10.1061/(ASCE)HY.1943-7900.0000373), 2011.

775 Kenney, T. A. (2006), Cross-sectional progression of apparent bedload velocities, in: Proceedings of the Eighth
776 Federal Interagency Sedimentation Conference (8th FISC), April 2–6 2006, Reno, Nevada, USA, 8 pp., 2006.

777 Kondolf, G. M., Schmitt, R. J. P., Carling, P., et al.: Changing sediment budget of the Mekong: Cumulative threats
778 and management strategies for a large river basin. *Sci Total Environ.*, 625, 114-134,
779 <https://doi.org/10.1016/j.scitotenv.2017.11.361>, 2018.

780 Kostaschuk, R., and Villard, P.: Flow and sediment transport over large subaqueous dunes: Fraser River, Canada,
781 *Sedimentology*, 43 (5), 849-863, <https://doi.org/10.1111/j.1365-3091.1996.tb01506.x>, 1996.

782 Kostaschuk, R., Best, J., Villard, P., Peakall, J., and Franklin, M.: Measuring flow velocity and sediment transport
783 with an acoustic Doppler current profiler, *Geomorphology*, 68, 25-37,
784 <https://doi.org/10.1016/j.geomorph.2004.07.012>, 2005.

785 Latosinski, F. G., Szupiany, R. N., Guerrero, M., Amsler, M. L., and Vionnet, C.: The ADCP's bottom track capability
786 for bedload prediction: Evidence on method reliability from sandy river applications, *Flow Measurement and*
787 *Instrumentation*, 54, 124-135, <https://doi.org/10.1016/j.flowmeasinst.2017.01.005>, 2017.

788 Leary, K. C. P., and Buscombe, D.: Estimating sand bed load in rivers by tracking dunes: a comparison of methods
789 based on bed elevation time series, *Earth Surf. Dynam.*, 8, 161-172, <https://doi.org/10.5194/esurf-8-161-2020>,
790 2020.

791 Le Guern, J., Rodrigues, S., Tassi, P., Jugé, P., Handfus, T., Duperray, A., and Berrault, P.: Influence of migrating
792 bars on dune geometry, in: *Book of Abstracts of the 6th Marine and River Dune Dynamics conference*, 1-3 April
793 2019, Bremen, Germany, 157-160, 2019a.

794 Le Guern, J., Rodrigues, S., Tassi, P., Jugé, P., Handfus, T., and Duperray, A.: Initiation, growth and interactions
795 of bars in a sandy-gravel bed river, in: *Book of Abstracts of the 11th Symposium on River, Coastal and Estuarine*
796 *Morphodynamics*, 16-21 November 2019, Auckland, New-Zealand, 226 pp., 2019b.

797 Marineau, M. D., Wright, S. A., and Gaeuman, D.: Calibration of sediment-generated noise measured using
798 hydrophones to bedload transport in the Trinity River, California, USA, in: *Proceeding of River Flow 2016 - eighth*
799 *International Conference on Fluvial Hydraulics*, Saint Louis, USA, 12-15 July 2016, 1519–1526, 2016.

800 Mendoza, A., Abad, J. D., Langendoen, E. J., Wang, D., Tassi, P., and El Kadi Abderrezak, K.: Effect of Sediment
801 Transport Boundary conditions on the Numerical Modeling of Bed Morphodynamics, *J. Hydraul. Eng.*, 143 (4),
802 [https://doi.org/10.1061/\(ASCE\)HY.1943-7900.0001208](https://doi.org/10.1061/(ASCE)HY.1943-7900.0001208), 2017.

803 Nittrouer, J. A., Allison, M. A., and Campanella, R.: Bedform transport rates for the lowermost Mississippi River, *J.*
804 *Geophys. Res.*, 113, F03004, <https://doi.org/10.1029/2007JF000795>, 2008.

805 Peters, J. J.: Discharge and Sand Transport in the Braided Zone of the Zaire Estuary, *Netherlands Journal of Sea*
806 *Research*, 12, 273-292, [https://doi.org/10.1016/0077-7579\(78\)90031-5](https://doi.org/10.1016/0077-7579(78)90031-5), 1978.

807 Ramooz, R., and Rennie, C. D.: Laboratory Measurement of Bedload with an ADCP, U.S. Geological Survey
808 Scientific Investigations Report, 2010-5091, 2010.

809 Reesink, A. J. H., Parsons, D. R., and Thomas, R. E.: Sediment transport and bedform development in the lee of
810 bars: Evidence from fixed- and partially-fixed bed experiments, in: Proceeding of River Flow 2014 - seventh
811 International Conference on Fluvial Hydraulics, Lausanne, Switzerland, 3-5 Septembre 2014, 8 pp., 2014.

812 Rennie, C. D., and Millar, R. G.: Measurement of the spatial distribution of fluvial bedload transport velocity in both
813 sand and gravel, *Earth Surf. Process. Landforms*, 29, 1173-1193, doi:10.1002/esp.1074, 2004.

814 Rennie, C. D., and Villard, P. V.: Site specificity of bed load measurement using an acoustic Doppler current profiler,
815 *J. Geophys. Res.*, 109, F03003, <https://doi.org/10.1029/2003JF000106>, 2004.

816 Rennie, C. D., Millar, R. G., and Church, M. A.: Measurement of Bed Load Velocity using an Acoustic Doppler
817 Current Profiler, *J. Hydraul. Eng.*, 128 (5), 473-483, [https://doi.org/10.1061/\(ASCE\)0733-9429\(2002\)128:5\(473\)](https://doi.org/10.1061/(ASCE)0733-9429(2002)128:5(473)),
818 2002.

819 Rennie, C. D., Vericat, D., Williams, R. D., Brasington, J., and Hicks, M.: Calibration of acoustic doppler current
820 profiler apparent bedload velocity to bedload transport rate, in: *Gravel-Bed Rivers: Processes and Disasters*,
821 Oxford, UK: Wiley Blackwell, 209–233, <https://doi.org/10.1002/9781118971437.ch8>, 2017.

822 Rodrigues, S., Mosselman, E., Claude, N., Wintenberger, C. L., and Jugé, P.: Alternate bars in a sandy gravel bed
823 river: generation, migration and interactions with superimposed dunes, *Earth Surf. Process. Landforms*, 40 (5),
824 610-628, <https://doi.org/10.1002/esp.3657>, 2015.

825 Simons, D. B., Richardson, E. V., and Nordin, C. F. Jr.: Bedload Equation for Ripples and Dunes, U.S. Geol. Survey
826 Prof. Paper, 462-H, <https://doi.org/10.3133/pp462H>, 1965.

827 Syvitski, J. P. M., and Milliman, J. D.: Geology, Geography, and Humans Battle for Dominance over the Delivery of
828 Fluvial Sediment to the Coastal Ocean, *The Journal of Geology*, 15(1), 1-19, <https://doi.org/10.1086/509246>, 2007.

829 Ten Brinke, W. B. M., Wilbers, A. W. E., and Wesseling, C.: Dune growth, decay and migration rates during a large-
830 magnitude flood at a sand and mixed sand-gravel bed in the Dutch Rhine river system, in: *In Fluvial Sedimentology*
831 VI, Vol. 28 of Special Publications of the International Association of Sedimentologists, 15-32,
832 <https://doi.org/10.1002/9781444304213.ch2>, 1999.

833 Thorne, P. D., Heathershaw, A. D., and Troiano, L.: Acoustic Detection of Seabed Gravel Movement in Turbulent
834 Tidal Currents, *Marine Geology*, 54, M43-M48, [https://doi.org/10.1016/0025-3227\(84\)90035-5](https://doi.org/10.1016/0025-3227(84)90035-5), 1984.

835 Thorne, P. D.: The measurement of acoustic noise generated by moving artificial sediments, *J. Acoust. Soc. Am.*,
836 78 (3), 1013–1023, <https://doi.org/10.1121/1.393018>, 1985.

837 Thorne, P. D.: Laboratory and marine measurements on the acoustic detection of sediment transport, *J. Acoust.*
838 *Soc. Am.*, 80(3), 899, <https://doi.org/10.1121/1.393913>, 1986.

839 Thorne, P. D.: An overview of underwater sound generated by interparticle collisions and its application to the
840 measurements of coarse sediment bedload transport, *Earth Surf. Dyn.*, 2 (2), 531–543,
841 <https://doi.org/10.5194/esurf-2-531-2014>, 2014.

842 Van den Berg, J. H.: Bedform migration and bed-load transport in some rivers and tidal environments,
843 *Sedimentology*, 34, 681-698, <https://doi.org/10.1111/j.1365-3091.1987.tb00794.x>, 1987.

844 Van der Mark, C. F., and Blom, A.: A new and widely applicable tool for determining the geometric properties of
845 bedforms, Civil Engineering & Management Research Report 2007R-003/WEM-002 ISSN 1568-4652, University
846 of Twente, Enschede, Netherlands, 57 pp., 2007.

847 Van Rijn, L. C.: Sediment Transport. Part I: Bed Load Transport, *J. Hydraul. Eng.*, 110, 1431-1456,
848 [https://doi.org/10.1061/\(ASCE\)0733-9429\(1984\)110:10\(1431\)](https://doi.org/10.1061/(ASCE)0733-9429(1984)110:10(1431)), 1984.

849 Van Rijn, L. C., and Gaweesh, M. T. K.: New Total Sediment-Load Sampler, *J. Hydraul. Eng.*, 118 (12), 1686–
850 1691. [https://doi.org/10.1061/\(ASCE\)0733-9429\(1992\)118:12\(1686\)](https://doi.org/10.1061/(ASCE)0733-9429(1992)118:12(1686)), 1992.

851

852 Villard, P. V., and Church, M.: Bar and dune development during a freshet: Fraser River Estuary, British Columbia,
853 Canada, *Sedimentology*, 52, 737-756, <https://doi.org/10.1111/j.1365-3091.2005.00721.x>, 2005.

854 Villard, P., Church, M., and Kostaschuk, R.: Estimating bedload in sand-bed channels using bottom tracking from
855 an acoustic Doppler profiler, *Spec. Pubs int. Ass. Sediment*, 35, 197-209,
856 <https://doi.org/10.1002/9781444304350.ch12>, 2005.

857 Vörösmarty, C., McIntyre, P., Gessner, M., Dudgeon, D., Prusevich, A., Green, P., Glidden, S., Bunn, S. E.,
858 Sullivan, C. A., Reidy Liermann, C., and Davies, P. M.: Global threats to human water security and river biodiversity,
859 *Nature*, 467, 555–561, <https://doi.org/10.1038/nature09440>, 2010.

860 Wilbers, A.: The development and hydraulic roughness of subaqueous dunes, *Neth. Geogr. Stud, Fac. of Geosci.,*
861 *Utrecht Univ., Utrecht, Netherlands*. 323, 224 pp., 2004.

862 Williams, R. D., Rennie, C. D., Brasington, J., Hicks, D. M., and Vericat, D.: Linking the spatial distribution of bed
863 load transport to morphological change during high-flow events in shallow braided river, *J. Geophys. Res. Earth*
864 *Surf.*, 120, 604–622, <https://doi.org/10.1002/2014JF003346>, 2015.